

### TECHNICAL UNIVERSITY OF CIVIL ENGINEERING BUCHAREST DOCTORAL SCHOOL

### PhD THESIS SUMMARY

# Displacement-based design considering the seismic hazard in Romania

PhD Candidate: Adviser:

Ing. Paul Olteanu Prof. univ. dr. ing. Radu Văcăreanu

BUCHAREST 2022

### Contents

A	cknov	vledgements	3
Iı	ntrodu	ction	4
1	Displacement-based design methodologies		5
	1.1	Direct displacement-based seismic design - Priestley, Calvi & Kowalsky	6
	1.2	Displacement-based design, Chopra formulation	9
2	Crı	ustal and intermediate-depth earthquakes	11
3	Ground motion prediction equation (GMPE) for the displacement spectrum ordinates 13		
4	Ine	lastic displacement spectra	19
5	Use	e of overdamped spectra in the analysis of the expected seismic response	26
6	Cas	se studies	34
7	Conclusions		38
	7.1	Personal contributions	38
	7.2	Recommendations for future research	41
8	Pul	olished articles	42
R	References		

### Acknowledgements

The doctoral thesis was developed between 2015-2022, within the Technical University of Constructions of Bucharest, Faculty of Civil, Industrial and Agricultural Constructions.

I would like to express my sincere gratitude to my supervisor, Prof. Radu Văcăreanu, for his trust, guidance and encouragement throughout the completion of this thesis. I am deeply grateful for his introduction to advanced methods in the field of earthquake engineering and engineering seismology, always connected to the latest developments in the literature.

I want to express my gratitude to Prof. Loretta Batali, Prof. Marius Moșoarcă, Prof. Petru Mihai and Prof. Viorel Popa for their patience and competence with which they went through the thesis and for the suggestions made.

I thank Dr. Florin Pavel for giving me access to a large number of records, USDP software and for the support provided throughout the thesis preparation. To Dr. Cristian Neagu I am grateful for the information regarding the zoning of the Romanian territory by soil type, according to Eurocode 8.

I thank the National Research Institute for Earth Science and Disaster Resilience (NIED) for the permission to use the database of the Japanese K-NET and KiK-net networks.

I am grateful to Mr. Cristian Onofrei for his contributions in my training as a structural engineer and for encouraging me to pursue doctoral studies. I am deeply indebted to Dr. Florin Köpe for all the conversations we have had over the years on technical issues and for opening a door to a bigger world for me.

I would like to thank Dr. Tudor Saidel and Dr. Ion Răileanu for the fruitful discussions regarding soil dynamics and for giving me the opportunity to participate in the in situ testing a number of reinforced concrete column-pile assemblies, in a cyclic stress regime.

I would like to thank my colleagues, Dr. Veronica Colibă and Dr. Ionuț Crăciun, for the support and collegiality shown during the doctoral studies. I also thank my colleagues and friends: George Gherghiță, Tudor Golea, Robert Angheluț, Alex Popescu and Raluca Buzău who supported me during the elaboration of the thesis.

Last but not least, I would like to thank my dear wife, Florența, and my children, Alex and Ștefan, for their understanding, patience and encouragement over the years.

### Introduction

The aim of the thesis is to more accurately identify the displacement demand imposed by Vrancea intermediate-depth earthquakes on reinforced concrete structural systems with elastic or inelastic behavior, researching the opportunity to use overdamped spectra in assessing seismic response and finding a design methodology based on displacement control to offer economically advantageous solutions for sizing reinforced concrete structures in Romania.

Chapter 1 outlines the characteristic features of displacement-based design (DBD). The vulnerabilities of the traditional force-based design method are highlighted. The defining elements of seismic performance are described: levels and performance objectives and the limit states to be considered for DBD, along with the input data required to initialize the DBD procedures, the seismic response spectra and the key parameters that significantly influence them. Next, the design methodology based on displacement control is conceptually presented. The procedures proposed by Priestley, Calvi and Kowalsky (2007) and those authored by Chopra and Goel (2001) are presented. The first procedure is based on the equivalence of the MDOF system with one SDOF corresponding to the maximum response, having an increased period and damping to take into account the inelastic energy dissipation, introduced in the calculation by equivalent hysteretic damping. The second procedure was developed for SDOF systems and follows a well-established approach for determining the displacement imposed to the equivalent inelastic system, the inelastic spectra of constant ductility. Also, in Chapter 1 are described two methods for assessing the deformation capacity of reinforced concrete elements, an analytical one, based on the integration of curvatures and the concept of plastic hinge, and the second, an empirical method developed by processing data obtained by testing the elements of reinforced concrete. Finally, some developments and applications of displacement-based seismic design and assessment are presented.

Chapter 2 deals with the similarities and differences between crustal earthquakes and those of intermediate-depth. Among the crustal sources that affect the Romanian territory, the Banat source is studied together with the relevant characteristics for DBD. The following are some defining features for the focal mechanism of the Vrancea subcrustal source.

In Chapter 3, a ground motion prediction equation (GMPE) was developed for the displacement spectrum ordinates, associated with a seismic scenario, taking into account the inter-event and intra-event variability. The parameters of the seismic scenario required for the construction of the spectrum are: the magnitude of the earthquake, the epicentral distance and the type of soil. For this purpose, a database of records was assembled, containing recordings from intermediate-depth earthquakes that occurred in the Vrancea seismic area or in a similar seismic tectonic regime. The GMPE coefficients were obtained by two stage regression. After testing the relationship according to the methodologies presented in the literature, the retrodiction capacity of seismic events was investigated.

Chapter 4 deals with the development of inelastic displacement spectra using the method of amplification coefficient of elastic displacement of the SDOF. The hysteretic model of the SDOF system is the modified Takeda model, suitable for describing the behavior of reinforced concrete

structures during strong earthquakes. The variability associated with this parameter and that associated with the GMPE is propagated in the inelastic displacement spectrum, obtaining a probabilistic description of the displacement demand, corresponding to a given seismic event. The influence of the magnitude of the earthquake, the epicentral distance and the ground conditions on the amplification coefficient were investigated. Finally, the inelastic displacement spectrum is obtained for a given seismic scenario and displacement ductility.

Chapter 5 includes a study of overdamped displacement spectra. The energy dissipation that takes place in the plastic zones of the structures with inelastic behavior during strong earthquakes is modeled by additional viscous damping (hysteretic). Some displacement-based design methodologies use the hysteretic damping and the effective period of an equivalent system to estimate the displacement response of the actual structure. Two equivalent linearization procedures are tested, the predictions of the two being compared with the seismic response of the inelastic system described by the Takeda hysteretic model.

Chapter 6 presents the application of displacement-based seismic design for a number of structural systems located in various seismic areas in Romania. These were designed according to DBD and then successfully tested by nonlinear dynamic analysis, using a suite of recordings compatible with the design spectrum. Single story industrial structures with large height located in areas characterized by  $a_g = 0.30g$  and control periods  $T_C = 0.70s$  and  $T_C = 1.60s$ , single story industrial structures with moderate height on sites with  $a_g = 0.20g$  cu  $T_C = 0.70s$  and  $T_C = 1.00s$ . An eightstory building with structural reinforced concrete walls, and another one with a dual structure (frames and structural walls), both located in a seismic zone having  $a_g = 0.30g$  and control period  $T_C = 1.60s$  are also investigated.

The thesis ends with a chapter containing the conclusions, personal contributions and future directions of research.

### 1 Displacement-based design methodologies

The chapter aims to investigate the current state of the art in displacement-based design, the main developments and results presented in the literature. The aim was also to identify the levels and performance objectives, describe the load-deformation behavior of reinforced concrete elements using empirical and analytical methods (using the constitutive laws of materials and sectional analysis) and evaluate the stiffness of reinforced concrete structural elements.

Displacement-based design is a design methodology in which decisions are made taking into account structural deformations. Over time, a number of procedures have been developed that can be classified according to the role of deformations in the design, the type of structural analysis to be performed, the limitations of the structural system to which they can be applied and the limit states for which each method is suitable (FIB, 2003).

As far as the deformations are concerned in the design process, the DBD methods can consist in:

• checking the displacements/deformations of a pre-designed structure, modifying the reinforcement details until the deformation capacity exceeds the required one;

- an iterative sizing process, starting from a previously dimensioned structure but establishing a maximum limit of the displacement that will be imposed on the structure, the structural system being modified until the displacements are below the imposed limit;
- direct displacement-based design, starting from a predefined target displacement, the strength and rigidity of the structure being determined during the process, in order to maintain the displacements under control.

The direct displacement-based seismic design method developed by Priestley & Kowalsky in the 1990s, stands out in the family of displacement-based design methods because of its elegance and versatility.

1.1 Direct displacement-based seismic design - Priestley, Calvi & Kowalsky The method was developed in response to the limitations of current force-based design, limitations set out in detail in Priestley (2003). It is based on the description of the structure as a system with a single degree of dynamic freedom (SDOF), represented by the secant rigidity at the maximum response point, i.e., on the concept of substitute structure developed by Shibata & Sozen (1974).

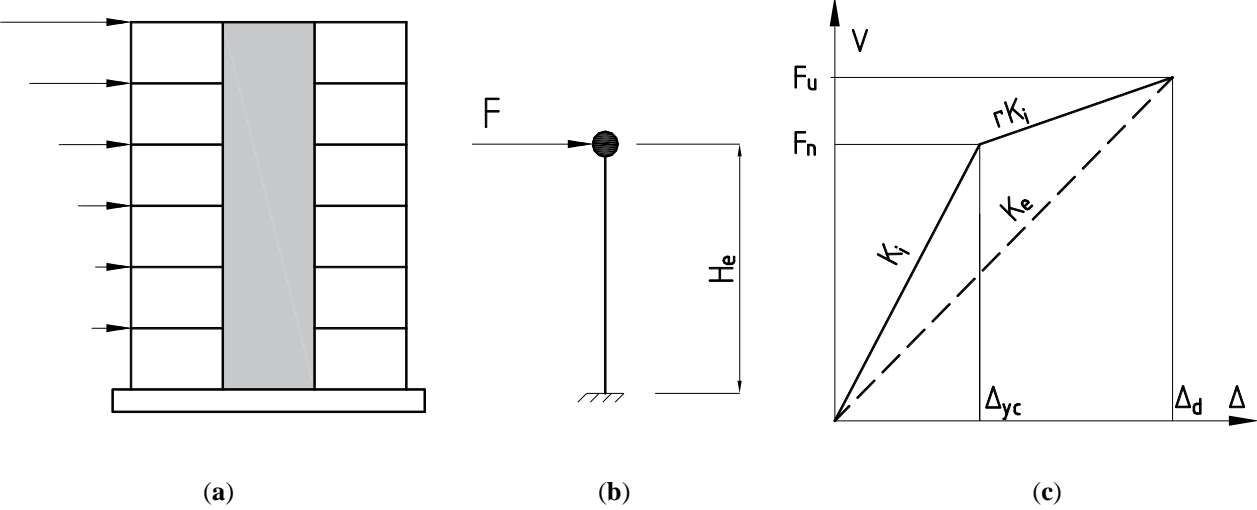


Fig. 1-1 MDOF transformation (a) to a SDOF system (b); effective stiffness (c), Priestley, Calvi & Kowalsky (2007).

The basic formulation (Priestley, Calvi & Kowalsky, 2007) consists in assimilating the multiple degree of freedom (MDOF) structure to a an equivalent SDOF system, having the stiffness equal to the secant at the maximum response point and increased viscous damping, in order to keep account for inelastic energy dissipation in the plastic zones of the structure, as shown in Figures 1-1 and 1-2. For the equivalent structure, the force-displacement curve is represented, composed of two straight segments, the first describing the elastic domain ( $K_i$  stiffness) and the second the plastic domain (having low stiffness,  $rK_i$ ).  $\Delta_d$ , the design displacement, it is the dependable displacement of the system for the chosen limit state and the hazard level considered. It is used to calculate the ductility of the substitute structure. Knowing the material and the structural type, an equivalent damping ratio can be determined.

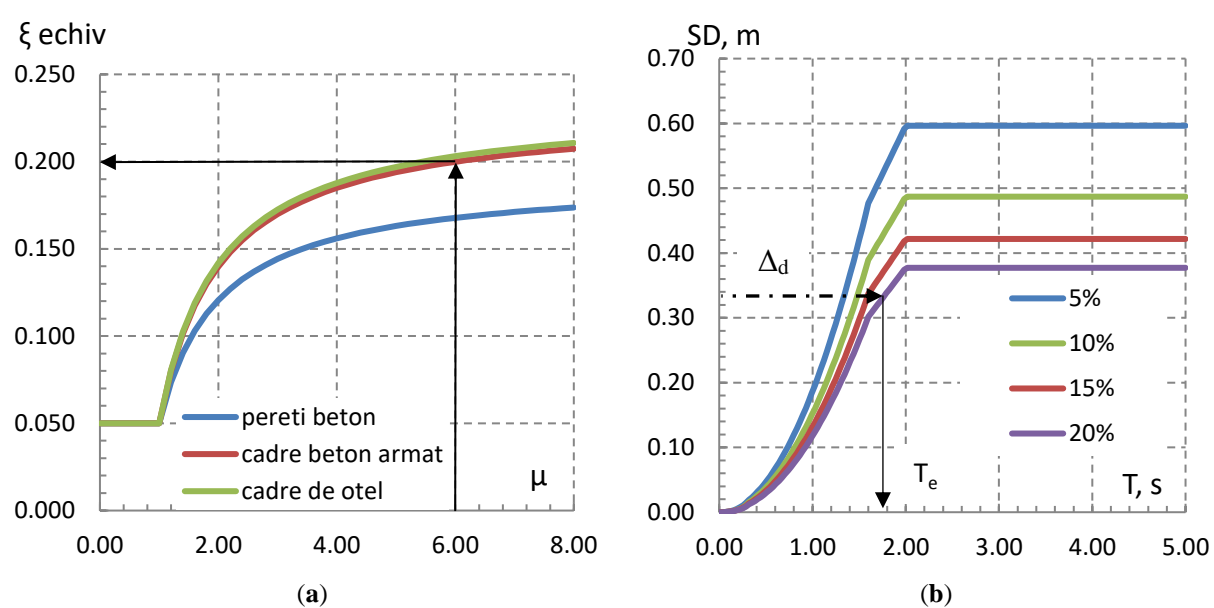


Fig. 1-2 Equivalent viscous damping, (Priestley, Calvi & Kowalsky, 2007) (a); design displacement spectrum (b)

Then, using displacement spectra, the actual period of the structure can be found (corresponding to the considered level of hazard). Knowing the vibration period, one can determine the equivalent rigidity and the base shear:

$$K_e = 4\pi^2 m_e / T_e^2$$

$$F = K_e \Delta_d$$
Ec. 1-1

where  $K_e$  is the effective stiffness of the SDOF system,  $m_e$  is the mass associated with the fundamental mode of vibration, and  $T_e$  is the vibration period corresponding to the maximum displacement imposed at the equivalent height  $H_e$ .

The concept of the method is simple, the difficulties begin to appear in determining the characteristics of the substitute structure, the design displacement ( $\Delta_d$ ) and in constructing the design spectra for the design corresponding to the expected displacement ductility. In the basic formulation, the different energy dissipation properties are decoupled from the displacement spectrum, the nonlinear behavior of the elements being captured by the equivalent damping (Priestley, Calvi & Kowalsky, 2007). The design displacement for a SDOF structure depends on the considered limit state and can be calculated according to the material strain limits associated with it. The material limit strains, corresponding to the considered limit state, are  $\varepsilon_{cls}$  (concrete), respectively  $\varepsilon_{sls}$  (reinforcement), and are not reached simultaneously. The associated limit curvatures are (Priestley, Calvi & Kowalsky, 2007):

$$\phi_{ls,c} = \frac{\mathcal{E}_{c,ls}}{c},$$

$$\phi_{ls,s} = \frac{\mathcal{E}_{s,ls}}{d-c},$$

$$\phi_{ls} = \min(\phi_{ls,c}, \phi_{ls,s})$$
Ec. 1-2

Design displacement for the SDOF system is:

$$\Delta_{d,ls} = \Delta_y + \Delta_p = \frac{\phi_y (H + L_{SP})^2}{3} + (\phi_{ls} - \phi_y) L_p H$$
 Ec. 1-3

where H is the height of the column,  $L_{SP}$  is the yield penetration length and  $L_p$  is the plastic hinge length. If there is a drift limitation,  $\theta c$ , specified in the code for the limit state:

$$\Delta_{d\theta} = \theta_c H$$

The smaller of the two displacements is the design displacement,  $\Delta_d$  (Priestley, Calvi & Kowalsky, 2007).

In order to calculate the design displacement and to estimate displacement ductility,  $\mu_{\Delta} = \Delta_d / \Delta_y$ , it is necessary to find the yield displacement. Analytical studies, described in Priestley (2003) and then experimentally verified, revealed that, for reinforced concrete elements, the yield curvature depends only on the sectional depth and the yielding strain of the reinforcement, changing slightly with axial force and the amount of reinforcement.

For a cantilever SDOF system, the yield displacement is:

$$\Delta_{y} = \frac{\phi_{y} (H + L_{SP})^{2}}{3}$$
 Ec. 1-5

The yielding curvature correspond to the intersection of a line passing through the point of first yield with a horizontal line corresponding to the nominal resistance capacity (Priestley, Calvi & Kowalsky, 2007).

The classical formulation of direct displacement-based design is centered on the concept of equivalent viscous damping. This creates the connection between displacement ductility and displacement demand. Equivalent viscous damping is a way of describing the behavior of a system with nonlinear behavior. Numerous studies cited in Blandon (2004) have started from the following equation to determine the total fraction of critical damping:

$$\xi_{eq} = \xi_{el} + \xi_{hvst}$$
 Ec. 1-6

the equivalent damping being considered as the sum of the 'elastic' damping,  $\xi_{el}$ , and the hysteretic damping,  $\xi_{hyst}$ . The first term to the right of the equation has the value 0,05 of the critical damping. The estimation of the second term is the key to the correct description of the behavior of a nonlinear system modeled by equivalent viscous damping.

Chapter 5 presents in detail significant results on hysteretic damping models found in the literature, their related parameters and the corresponding damping values.

In Priestley, Calvi & Kowalsky (2007) the following expressions are given for equivalent viscous damping:

$$\xi_{eq} = 0.05 + 0.444 \left(\frac{\mu - 1}{\mu \pi}\right)$$
 for structural walls

$$\xi_{eq} = 0.05 + 0.565 \left( \frac{\mu - 1}{\mu \pi} \right)$$
 for reinforced concrete frames

where  $\mu$  is the system displacement ductility.

The influence of damping with values higher than 5% of the critical damping, on the ordinates of the displacement spectra is taken into account through a correction factor (CEN, 2004):

$$\eta = \sqrt{10/(5 + \xi_{eq})}$$
 Ec. 1-9

### 1.2 Displacement-based design, Chopra formulation

The methodology was developed by Chopra and Goel in their 2001 paper, where they drew attention to design situations where the use of overdamped displacement spectra led to unconservative results (Chopra & Goel, 2001). Instead of overdamped spectra, inelastic spectra of constant ductility are used, which allow a rigorous description of the displacement requirement imposed on SDOF systems during strong earthquakes.

The calculation procedure starts from the initial steps described in (Priestley & Calvi, 1997). They consist of: (a) estimating the yield displacement of the SDOF system,  $\Delta_y$ ; (b) determination of a permissible plastic rotation, depending on the type of element, geometry, detailing and the intended level of seismic performance,  $\theta_p$ , see Figure 1-3 (a); (c) calculation of design displacement as the sum of yield and plastic displacement,  $\Delta_d$ ; (d) calculation of the displacement ductility of the SDOF system,  $\mu_{\Delta}$ ; (e) calculation of the vibration period of the elastic system for which, at the given ductility, the design displacement is obtained (Chopra & Goel, 2001); (f) obtaining the initial (elastic) stiffness of the SDOF system; (g) determination of the base shear associated at yielding, detailing the reinforced concrete section; (h) repeat steps (a) to (g) until the convergence of the solution is reached. It should be noted that the displacement ductility of the system is implicitly controlled by the permissible plastic rotations.

The limitations of the method are given by the lack of recommendations regarding MDOF systems, the distribution of the force between the structural elements, the proportioning of the structural elements or the way the structures with flexible foundations should be considered (FIB, 2003).

The advantages of the methodology are the conceptual simplicity, appealing to the familiar concepts of inelastic spectra, as well as the fact that the initial stiffness of the system also controls the response of the inelastic system. Theoretically, one can find sizes of structural elements that, at the same time, on one hand satisfy the requirements for limiting rotations to prevent structural degradation, and on the other hand the requirements for limiting drift according to the code. These issues are considered in Chapter 6.

The disadvantages of the method are related to the need to generate inelastic spectra for each hysteretic model and level of displacement ductility, these involving specialized software for performing nonlinear dynamic analyzes for each spectral period.

Figure 1-3 (a) shows the parameters required in the DBD procedure for a simple SDOF system. Figure 1-3 (b) shows the elastic and inelastic spectra for three levels of displacement ductility,  $\mu_{\Delta} = 2$ ,  $\mu_{\Delta} = 3$  and  $\mu_{\Delta} = 4$ , together with the way to determine the eigen period of a system with  $\mu_{\Delta} = 3$  and Takeda hysteretic model for a design displacement of 15cm, for the FOC286N07W component. It is important to note that elastic (including code) displacement spectra can be used to generate constant ductility inelastic displacement spectra using the procedures in Chapter 4.

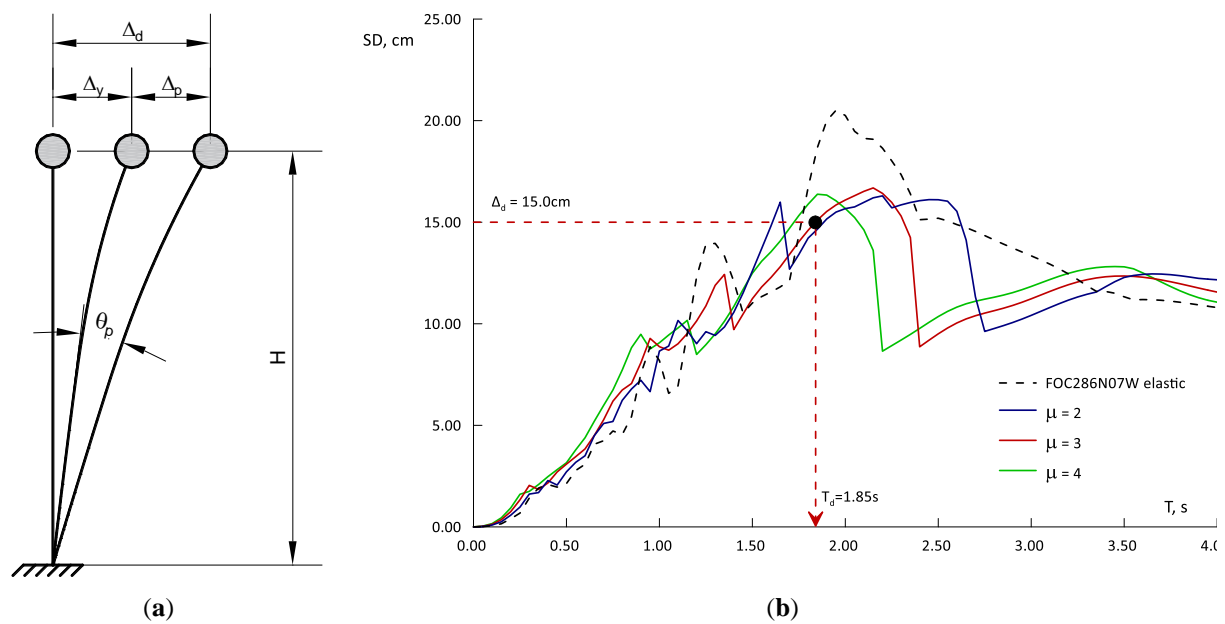


Fig. 1-3 SDOF system in displacement-based design (Chopra & Goel, 2001) (a), Chopra & Goel (2001) DBD for a system having  $\mu_{\Delta}=3$ ,  $\Delta_{d}=15cm$  using the FOC286N07W component (b)

Having determined the eigen period of the system with ductility  $\mu_{\Delta}$ , it is possible to determine the required stiffness, K, of the system at yielding:

$$K = \left(\frac{2\pi}{T_d}\right)^2 m$$
 Ec. 1-10

And the base shear, V<sub>y</sub>:

$$V_{\nu} = K\Delta_{\nu}$$
 Ec. 1-11

where m is the mass of the SDOF system,  $T_d$  is the structural period of the system for which the design displacement,  $\Delta_d$ , is recorded on the inelastic spectrum of displacement, while  $\Delta_y$  is the yield displacement.

Knowing the base shear at yielding of the SDOF system, one can proceed to the sizeing of the reinforced concrete sections. As mentioned above, the authors of the method did not detail how the seismic force is distributed over the height of the structure, or between the components of the

structure (walls of different lengths, for example). Also, the method is not customized for frame, wall or dual structures. However, a vertical distribution of seismic force proportional to mass and height can be adopted, while the distribution between structural walls of different lengths can be done iteratively, according to the shear stiffness at yielding (FIB, 2003). Chapter 6 presents calculations performed using this DBD methodology for single story industrial structures, wall and dual structures, subsequently verified by nonlinear dynamic analysis.

### 2 Crustal and intermediate-depth earthquakes

The objective of this chapter is to identify the similarities and differences between crustal earthquakes and those of intermediate-depth.

Depending on the depth at which they occur, earthquakes can be classified as crustal (with focal depth less than 60km), intermediate-depth earthquakes (subcrustal, with foci at 60-300km) and deep earthquakes (occurring at depths below 300km). Usually, subcrustal earthquakes occur in subduction zones, in the tectonic plate that sinks into the asthenosphere and are associated with volcanic activity. The characteristics by which subcrustal earthquakes differ from crustal ones are the absence of surface waves (or their limitation in intensity and duration), the more pronounced presence of volume waves along with a smaller number of aftershocks.

In the following figures the acceleration and displacement spectra are compared for two earthquakes of the same magnitude,  $M_W = 5.4$ , one crustal (recorded on November 22, 2014, with a depth of 40,9 km) and another of intermediate-depth (produced on April 25, 2009, 109,6km) for two locations, INCERC Bucharest and Giurgiu. Epicentral distances and local conditions are similar (for site class, please see Chapter 3).

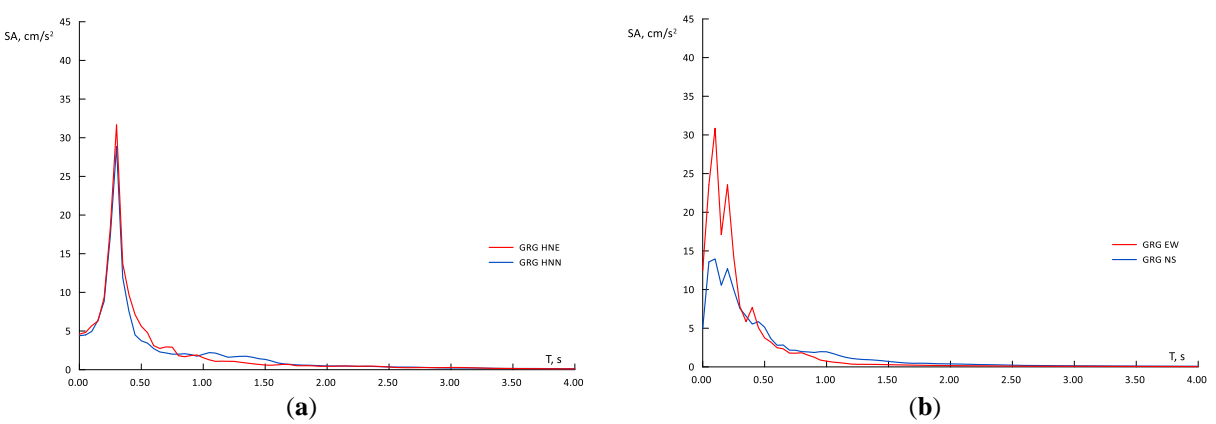


Fig. 2-1 Acceleration spectra for Giurgiu station: crustal (a) vs. intermediate-depth (b)

Figure 2-1 shows the acceleration spectra for Giurgiu station and the two earthquakes. There are very large amplifications present in the acceleration spectrum of the crustal earthquake in Giurgiu station, located around the period of 0.3s. The acceleration spectrum of the intermediate-depth earthquake envelopes over extended intervals the spectrum corresponding to the crustal earthquake, for both stations, as expected, taking into account the higher amplitudes of the ground acceleration in case of subcrustal earthquake.

Figure 2-2 examines the influence of earthquake type in terms of displacement spectra. The very small values of the maximum spectral displacements, less than 0.25 cm, are highlighted. Close values of spectral displacements are found for both locations and both earthquakes. Taking into account the much lower values of the ground acceleration for Giurgiu station compared to those recorded at INCERC station, this result is counterintuitive, possibly influenced by local geology. It is observed that the acceleration and displacement spectra corresponding to intermediate earthquakes exceed those of crustal earthquakes, for spectral periods between 0 and 1,5-2,0 s, after which the ordinates are comparable. This peculiarity was also highlighted in the study of Kanno et al. (2006). It is highlighted that the differences in attenuation for the two types of earthquakes are caused by the reflection and refraction of seismic waves in the Mohorovičić discontinuity.

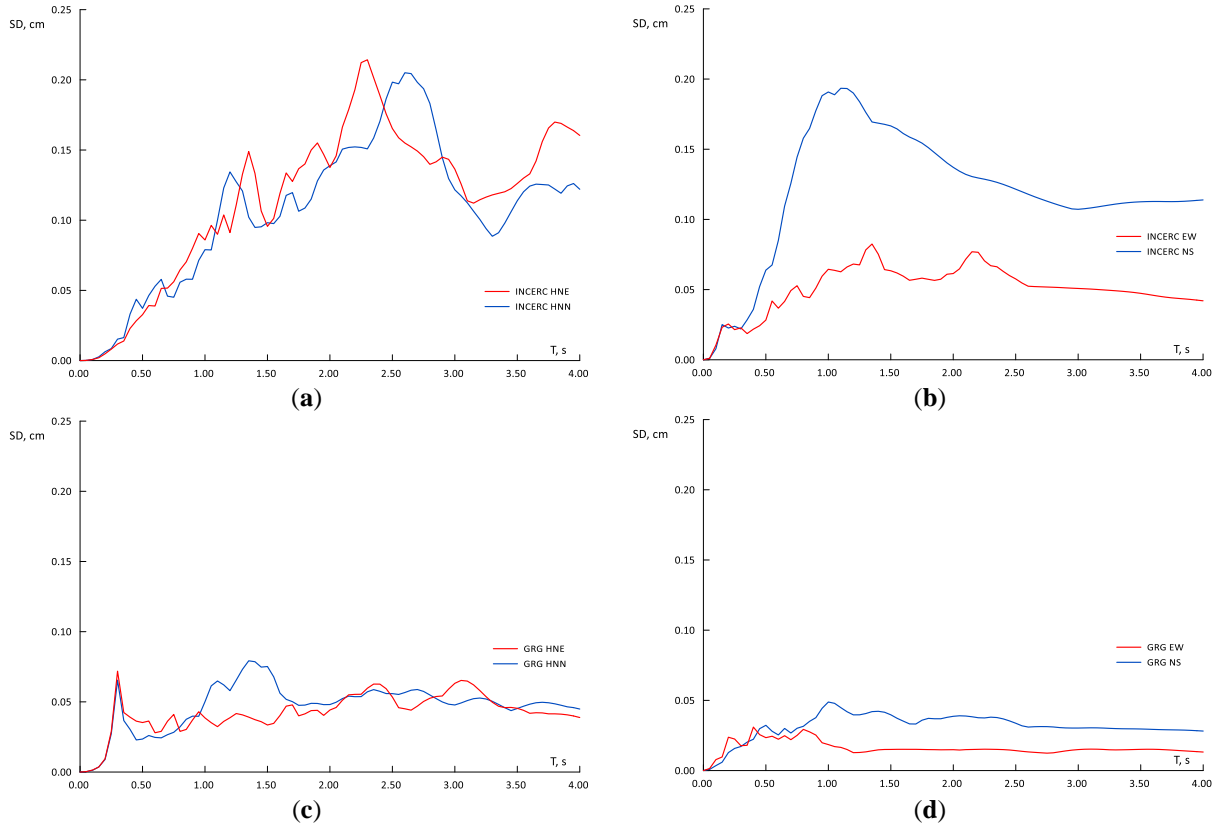


Fig. 2-2 Displacement spectra: crustal (a) INCERC, (c) Giurgiu vs. intermediate-depth (b) INCERC, (d) Giurgiu

Due to the small number of records of moderate - strong seismic events of crustal earthquakes, produced in other seismic areas than Vrancea, it was not considered appropriate to develop a GMPE for this type of earthquake. Attenuation models found in the literature, for example Cauzzi & Faccioli (2008), are calibrated for crustal earthquakes.

## 3 Ground motion prediction equation (GMPE) for the displacement spectrum ordinates

The objectives of this chapter are to assemble a database containing seismic recordings representative of the Vrancea intermediate-depth seismic source and to obtain the displacement spectrum using a GMPE built for this purpose, applicable in Romania, in the areas located in front of the Carpathian Arch, affected by the Vrancea subcrustal source.

The reason why it was considered appropriate to obtain displacement spectra by direct processing of records and not by deriving them from acceleration response spectra is that displacement spectra vary more strongly with magnitude than acceleration spectra. Moreover, the shape and ordinates of the displacement spectra are much more sensitive to the way the processing/correction of the records was done than the ordinates of the acceleration spectrum. The soil amplification caused by the local soil conditions are included implicitly in the model.

In order to develop the GMPE, a database of ground-motion records was assembled. The database used for this purpose comprises 272 pairs of records (544 horizontal components) from 15 earthquakes. The database includes only intermediate-depth earthquakes, nine of which occurred in the Vrancea area (235 pairs of records) while six earthquakes were recorded in Japan. The earthquakes in the database are in the range of magnitudes  $5,2 \le M_W \le 7,4$  and occurred at depths between 65 and 160 km, the database partially overlapping with that used in the study Văcăreanu, Radulian, Iancovici, Pavel & Neagu, (2015). Of the total records, 169 are from type C soil (approximately 62%), the rest were recorded on seismic stations located on type B ground. Soil classification was performed according to Eurocode 8. Digital recordings represent 52% of the total and are provided by earthquakes. with  $5,2 \le M_W \le 7,1$ . Therefore, most earthquakes in the database with  $M_W > 7,0$  were recorded analogously in Romania. The composition of the database by origin, ground type, magnitude and distance are shown in Figure 3-1.

In this study, Eurocode 8 classification was used for soil type classification (CEN, 2004). The shear wave speed is the weighted average for the layers located in the first 30m. It has the advantage that it is an established method (used in countries with a tradition in seismic action design), recommended by the national seismic design code, and can be applied relatively easily.

The GMPE ordinates of the relative displacement spectrum was obtained by two stage regression, using the methodology described in Joyner & Boore (1993) and Joyner & Boore (1994). Two stage regression is used to decouple the determination of the magnitude scaling from the determination of the distance scaling. The method is widely used in determining the coefficients of ground motion models, along with the algorithm developed by Abrahamson & Youngs (1992). Together with two-stage regression, Joyner and Boore introduced in the same article a one-stage regression method, the coefficients controlling the magnitude dependence and the distance dependence being determined simultaneously. Both methods are based on maximizing the likelihood of the set of observations.

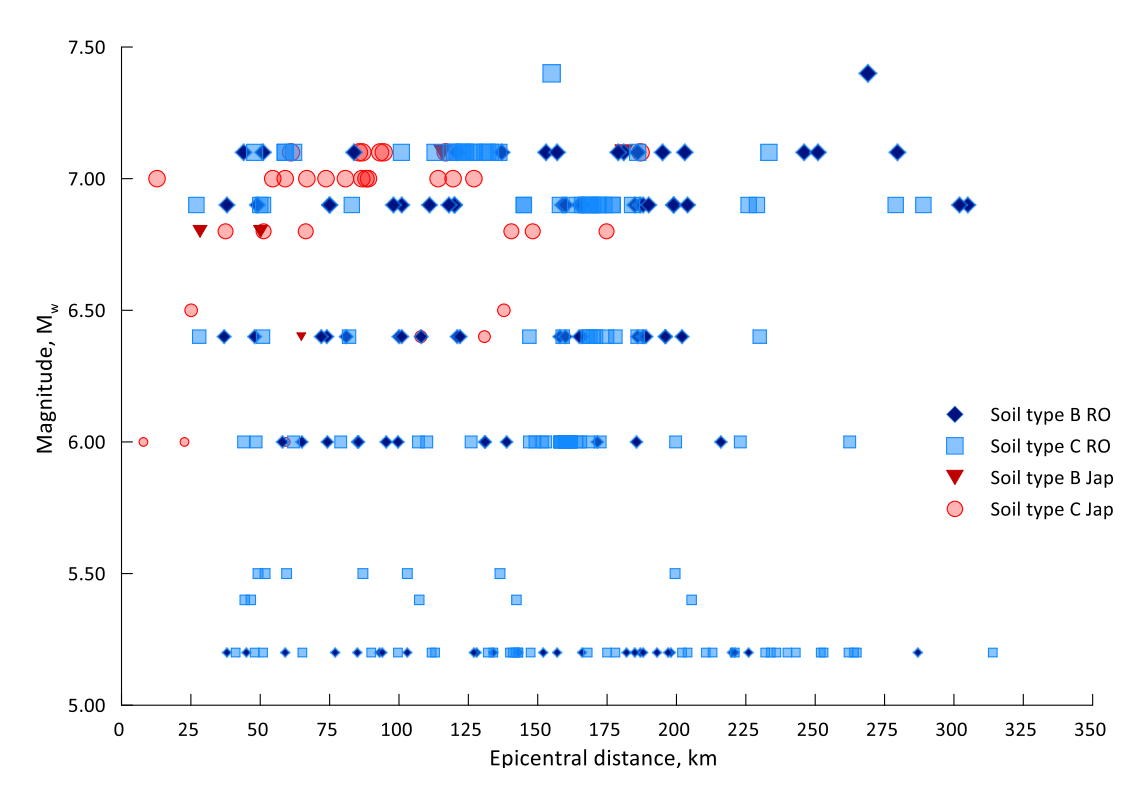


Fig. 3-1 Distribution by origin, ground type, magnitude and distance of records in the database

The two-stage regression consists first in determining the coefficients expressing the distance dependence and a vector of deviations (for each recording separately). In the second stage, the coefficients that express the dependence of the magnitude are determined by maximizing the likelihood of the set of observations.

The functional form of the ground motion model, adapted after Joyner & Boore, (1993) is:

$$\lg(SD) = a + b(M_W - 6) - \lg \sqrt{D_{epi}^2 + h^2} + c\sqrt{D_{epi}^2 + h^2} + \varepsilon_r + \varepsilon_e$$
 Ec. 3-1

where SD (in cm) is the ordinate of the elastic spectrum of relative displacements (geometric mean of two perpendicular horizontal components) for 5% damping,  $M_W$  is the moment magnitude of the earthquake,  $D_{epi}$  (in km) is the epicentral distance, a, b, c and h are coefficients that are determined by regression,  $\epsilon_r$  is a normally distributed independent random variable that takes values for each record,  $\epsilon_e$  is a normally distributed independent random variable that takes values for each earthquake and lg means logarithm in base 10. The random variable  $\epsilon_r$  has the mean 0 and the dispersion  $\sigma^2_r$ , representing the variability between the seismic stations (intra-event), while the random variable  $\epsilon_e$  has the average 0 and the dispersion  $\sigma^2_e$ , representing the variability between the seismic events (inter-event). The total standard deviation is:

$$\sigma = \sqrt{\sigma_c^2 + \sigma_e^2}$$
 Ec. 3-2

The first two terms of the attenuation relation take into account the quasi-linear variation of the logarithm of displacement the amplitude with the earthquake magnitude. The third term corresponds to the geometric attenuation of seismic waves, which decrease in proportion to the

inverse of the distance. The fourth term corresponds to anelastic attenuation, due to the geological layers traversed by seismic waves.

The GMPE's coefficients were determined separately for type B soil and type C soil, due to the much lower values of the spectral ordinates and to the difference between the spectral shapes for type B soils, as shown in Figure 3-2.

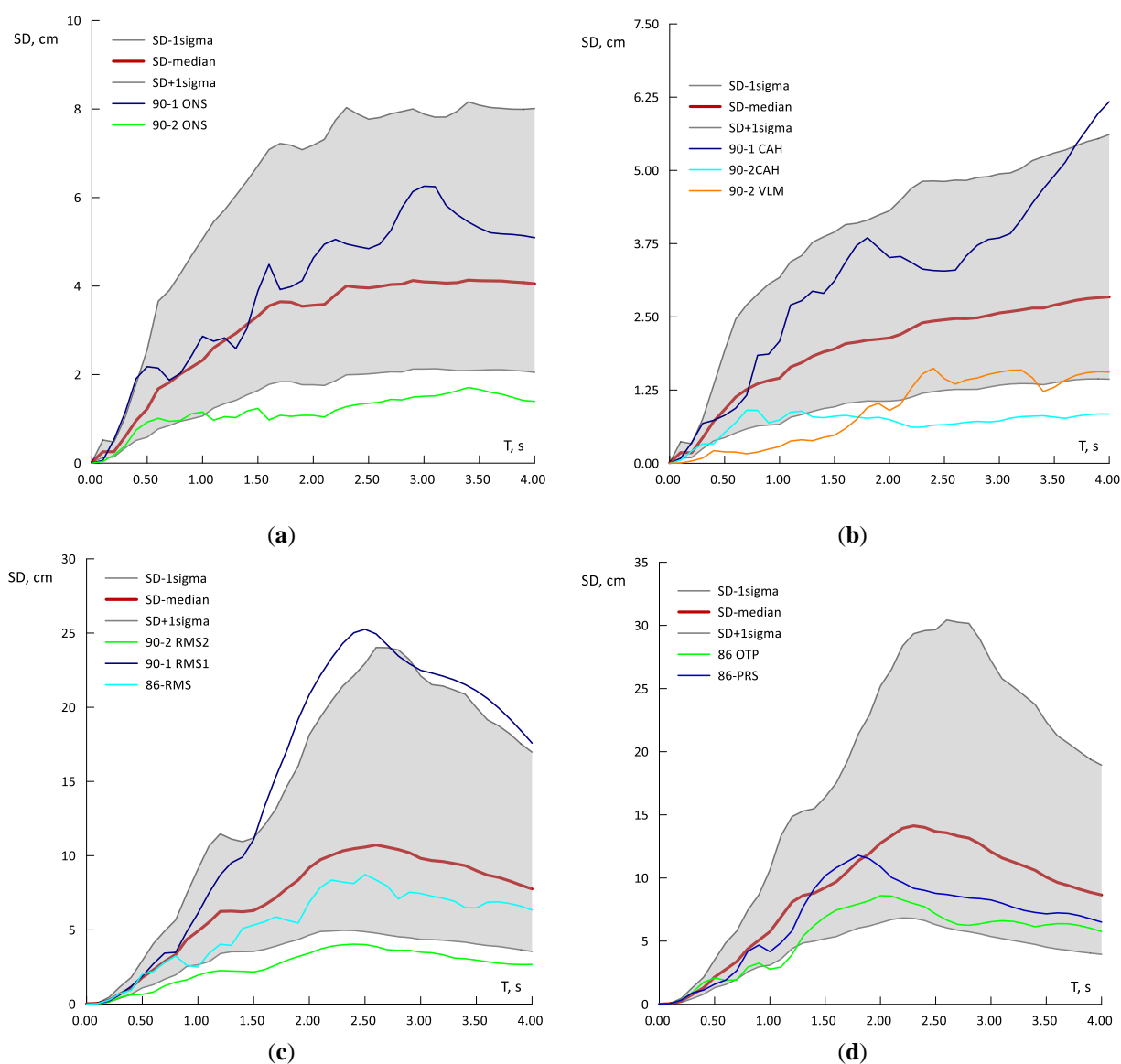


Fig. 3-2 Displacement spectra: from GMPE vs. calculated from records (a) soil type B, 50km; (b) soil type B, 100km; (c) type C ground 50 km; (d) type C ground 100km.

In order to improve the prediction of the response for large magnitude earthquakes ( $M_W > 7,1$ ), the opportunity to add a quadratic term to the basic attenuation relationship was explored, the GMPE reaching the following form:

$$\lg(SD) = a + b(M_W - 6) + d(M_W - 6)^2 - \lg\sqrt{D_{epi}^2 + h^2} + c\sqrt{D_{epi}^2 + h^2} + \varepsilon_r + \varepsilon_e$$
 Ec. 3-3

which indeed led to improved predictions for the March 4, 1977 earthquake and to some extent reduced residual values.

To investigate the database dependence of the ground motion model, the regression was performed on three data sets, one containing only strong national records from 1977, 1986 and 1990 earthquakes, the second data set consisted only of digital records (national, with  $5.2 \le \text{Mw} \le 6.0$  and Japanese, from the Kik-Net and K-NET networks, with  $6.0 \le \text{Mw} \le 7.1$ ) and the coefficients were determined up to periods of 8s and, and finally, one that contains recordings of all earthquakes in the database, with regression coefficients calculated in the range of 0.1 - 4.0s. Only the results corresponding to the first set will be presented below.

The set of moderate and strong national records, represented by earthquake records of 4 March 1977 ( $M_W = 7,4$ ), 31 August 1986 ( $M_W = 7,1$ ), 30 May 1990 ( $M_W = 6,9$ ) and 31 May 1990 ( $M_W = 6,4$ ), has as a main feature the high displacement demand imposed on tall structures (T > 1,0s) located on type C soil, a characteristic also observed in historical earthquakes. Figure 3-2 shows the predictions of displacement spectra for records in the database together with calculated SD, as the geometric mean of the two horizontal components of the recordings.

Using the GMPE (median values), the variation of the displacement spectra with the magnitude, the type of soil and the epicentral distance was analyzed. There is a tendency of narrowing the zone of large amplifications on the displacement spectrum with increasing earthquake magnitude, especially for ground type C. Smaller magnitude earthquakes tend to have quasi-flat areas over an extended range of periods, as confirmed by the calculated displacement spectra using earthquake records from 1986 and 1990. There are very high values of the relative amplification between the expected spectral values on the ground C and B, respectively. These are reduced to values found in the literature, for moderate earthquake magnitudes (Cauzzi & Faccioli, 2008). These high amplification values are confirmed by SD calculated using records from seismic stations located at the same epicentral distance, for the 1986 and 1990 earthquakes. For smaller magnitudes,  $M_W \leq 6.5$ , there is only a small increase (15-30 %) of displacement for sites located on type C ground in relation to type B sites. There are also large differences between the displacement demands between earthquakes separated by one degree of moment magnitude, as can be seen in Figure 3-3.

The variation with the epicentral distance is analyzed in Figure 3-4. For soil type C, the steep peak in the vicinity of the 2.30s period has a slight tendency to migrate to longer periods as the epicentral distance increases. The type B ground exhibits much lower values of spectral displacements, with a pronounced peak around the period of 1,80s followed by a relatively flat area. From Figure 3-4 it can be seen that for a increase by 50km of the epicentral distance the values of the spectral displacements decrease by 1/3. Also, increasing the epicentral distance has the effect of smoothing the spectral shape.

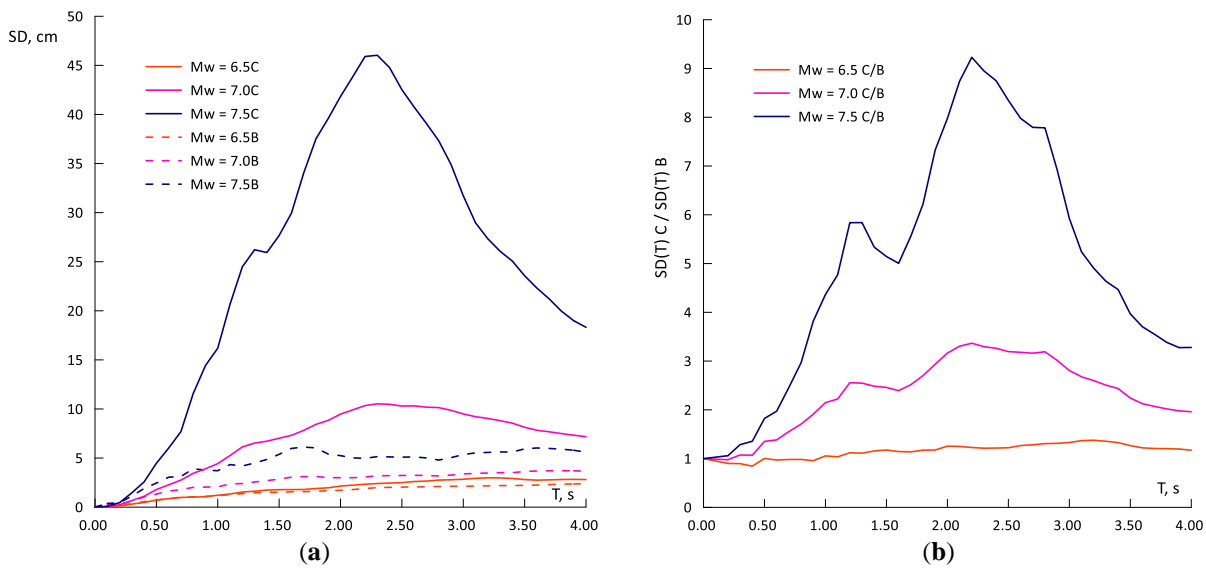


Fig. 3-3 Displacement demand as a function of magnitude and soil type (a) Displacement spectrum vs. earthquake magnitude,  $D_{epi}$ =100km and (b) Ratio between type C and type B displacement spectra,  $D_{epi}$  = 100km.

Figures 3-5 and 3-6 show the GMPE attenuation as a function of epicentral distance along with a comparison with two other attenuation laws for the elastic displacement spectrum, Cauzzi & Faccioli (2008) and Hassani, Amiri, Bararnia & Sinaeian (2017). Unfortunately, the two attenuation models are calibrated for crustal earthquakes.

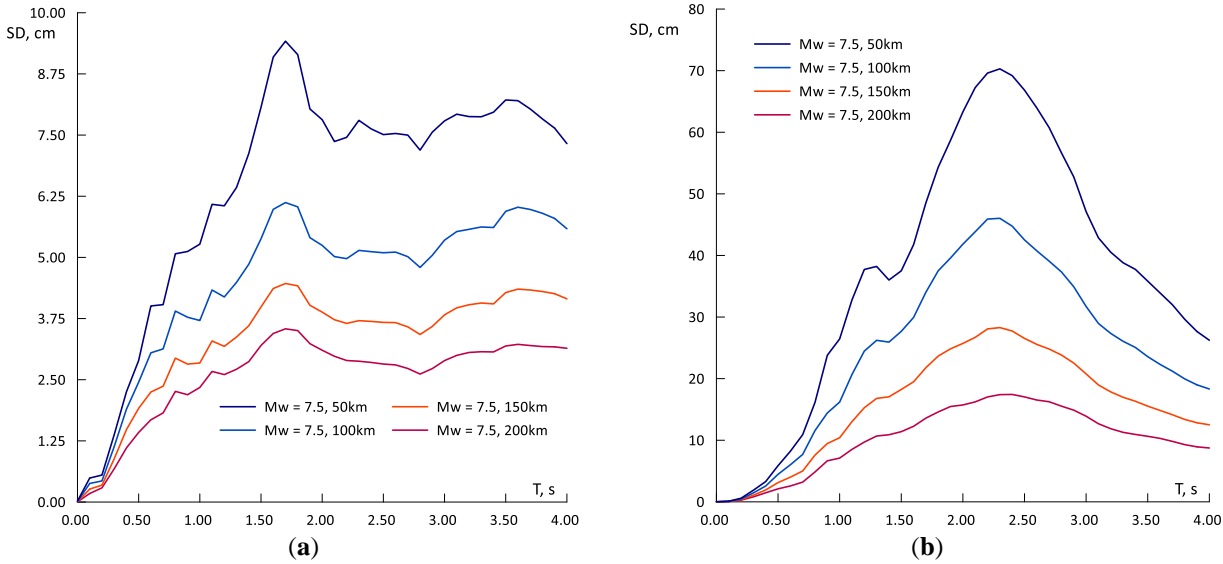


Fig. 3-4 Displacement spectra for an Mw=7.5 earthquake at 50, 100, 150, 200km epicentral distance. (a) soil type B; (b) soil type C

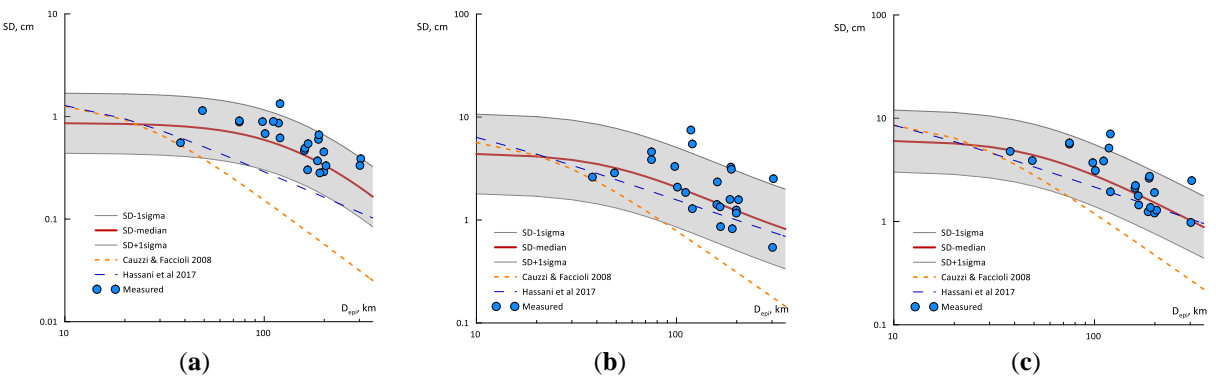


Fig. 3-5 GMPE attenuation with distance, type B soil (a) T=0,30s; (b) T=1,00s (c) T=1,50s

The amplitudes provided by the proposed ground motion model are marked with a red line, the gray band is an area bounded by  $\pm$  one standard deviation from the median values. For type B soils the proposed model provides similar results to the model proposed by Hassani et al, especially for the 1,0 and 1,5 s spectral periods, while the Cauzzi & Faccioli model attenuates the amplitudes at a higher rate. For locations located on type C soil the attenuation with the distance of the proposed model is more pronounced than for type B soil, for epicentral distances greater than 100km and almost non-existent for distances less than 100km, for all three periods analyzed. These results are in good agreement with the results from the application of the model by Vacareanu, Radulian, Iancovici, Pavel & Neagu (2015), which shows a very limited reduction for the amplitudes of spectral accelerations and distances below 100km. The attenuation of the proposed model differs significantly from that resulting from the application of the other two GMPEs. In the Cauzzi & Faccioli model, the amplitudes are attenuated more strongly, while the Hassani et al model leads to a nearly constant attenuation with increasing distance.

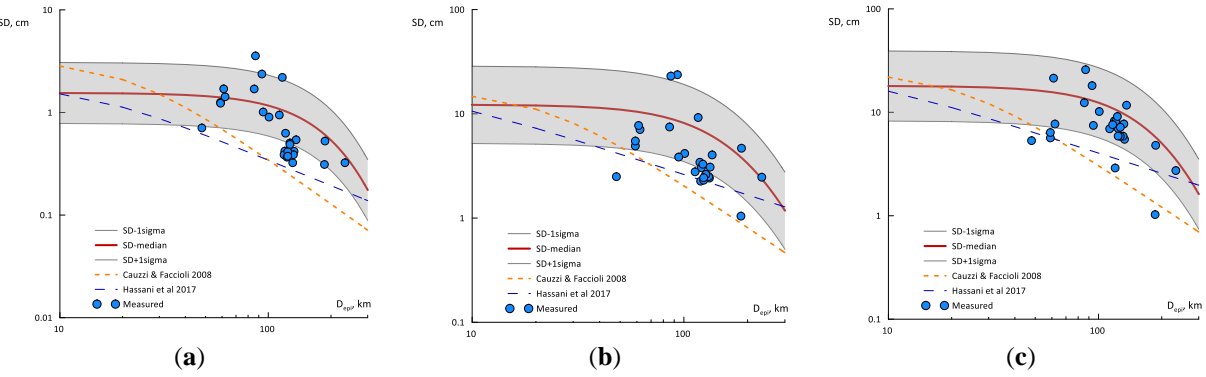


Fig. 3-6 GMPE attenuation with distance, type C soil (a) T=0,30s; (b) T=1,00s (c) T=1,50s

As can be seen, the proposed model constrains well the data obtained on type B soil. For locations located on type C soil, there is a group of records obtained at almost the same epicentral distance (seismic stations in Bucharest and surroundings) for which the attenuation model overestimates values of spectral displacements at periods of 0,3s and 1,0s. Given that the data deviating slightly from the predicted values are very localized (in space) and that the represented data come from only two earthquakes, the situation is not representative for the whole range of magnitudes and epicentral distances covered by the proposed model.

### 4 Inelastic displacement spectra

The objective of this chapter is to evaluate the displacement requirements of SDOF inelastic systems using the coefficient's method, expressed as a function of displacement ductility of the system,  $\mu$ . Using a database of strong seismic recordings, the amplification coefficient of elastic displacement, corresponding to a given hysteretic material/model, can be obtained through a statistical analysis of the ratio between inelastic and elastic displacements of the oscillator. The study focuses on new reinforced concrete structures, the hysteretic model being the modified Takeda model, with stiffness degradation.

In the displacement-based design calculation procedure, by using the displacement spectra for constant ductility, one of the intermediate steps is eliminated, resulting in a slightly simplified calculation mode. The conceptual advantage is that there is no need to make use of the concept of equivalent hysteretic damping, criticized by some researchers (Chopra & Goel, 2001), (Goel, 2018).

By associating the attenuation law presented in Chapter 3 with the results of this study, inelastic displacement spectra can be created for a given seismic scenario.

For this study, the PGA limit value was selected at  $75 \text{cm/s}^2$ , corresponding to the value of the geometric mean of the two horizontal components, according to the good practice recommendations from Goda and Atkinson (2009). The database includes 107 pairs of horizontal components (214 records) from intermediate-depth earthquakes produced in Romania and Japan, with  $6.0 \le \text{Mw} \le 7.40$ . Also included were two recordings of an earthquake with a magnitude of 5,2 (recorded in Romania on October 6, 2013), which meet the imposed PGA limit. The records were grouped according to the type of soil on which they were recorded, according to Eurocode 8 classification. Out of a total of 214 records, 140 came from type C soil, the remaining 74 from ground type B.

Nonlinear dynamic analyzes performed on SDOF systems were performed with the USDP computer software (Akkar, 2016). The amplification coefficient was calculated:

$$C_{\mu}(T) = \frac{SD_{inel}(T)}{SD_{el}(T)}$$
 Ec. 4-1

for all the 214 records, for periods between 0,05s and 4,00s in increments of 0,05s, for six displacement ductility values: 1,5, 2,0, 3,0, 4,0, 5, 0 and 6,0.  $SD_{inel}(T)$  is the inelastic displacement of a SDOF system with period T and displacement ductility  $\mu$ , while  $SD_{el}(T)$  represents the elastic displacement of the associated elastic system.

It is known that the seismic response of structures is influenced by local soil conditions (Aldea, 2013). Modern design codes take this influence into account, usually through a parameter describing the physical properties of the geological stratification corresponding to the site, such as the shear waves speed,  $v_{s,30}$ . The type of soil influences the displacement response of the structural system. In order to highlight the differences in displacement demand for structures located on soil type B and soil type C, the ratio between the median values of  $C_{\mu}(T)$  for ground type B and C, and

the corresponding median values for ground B and C were calculated (Miranda & Ruiz Garcia, 2003). Figure 4-1 shows that ignoring the type of ground is conservative for type B soil and periods up to 1,20s. For type C soil, the situation is reversed. The differences are accentuated by the increase in displacement ductility, but is not exceeding 10%. The values are consistent with those presented in the study of Miranda & Ruiz Garcia, (2003), which reports differences of 10-15% for type B ground and a maximum of 20% for type C soil. However, it should be noted that the database contained an equal number of records for three categories of soil, A, B, C.

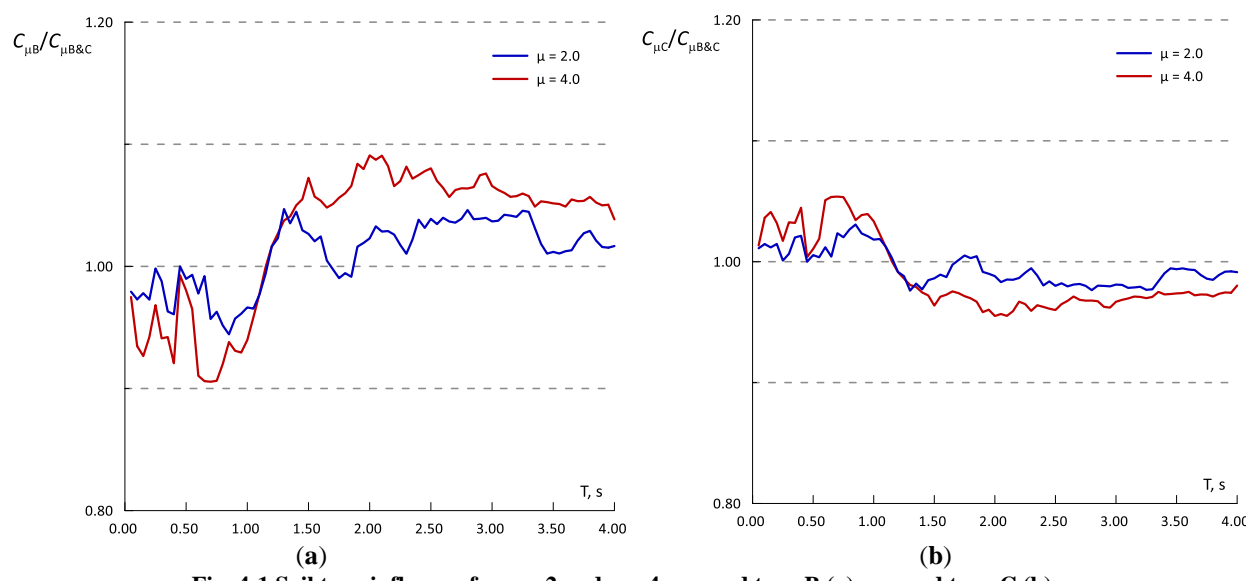


Fig. 4-1 Soil type influence for  $\mu$  = 2 and  $\mu$  = 4: ground type B (a); ground type C (b)

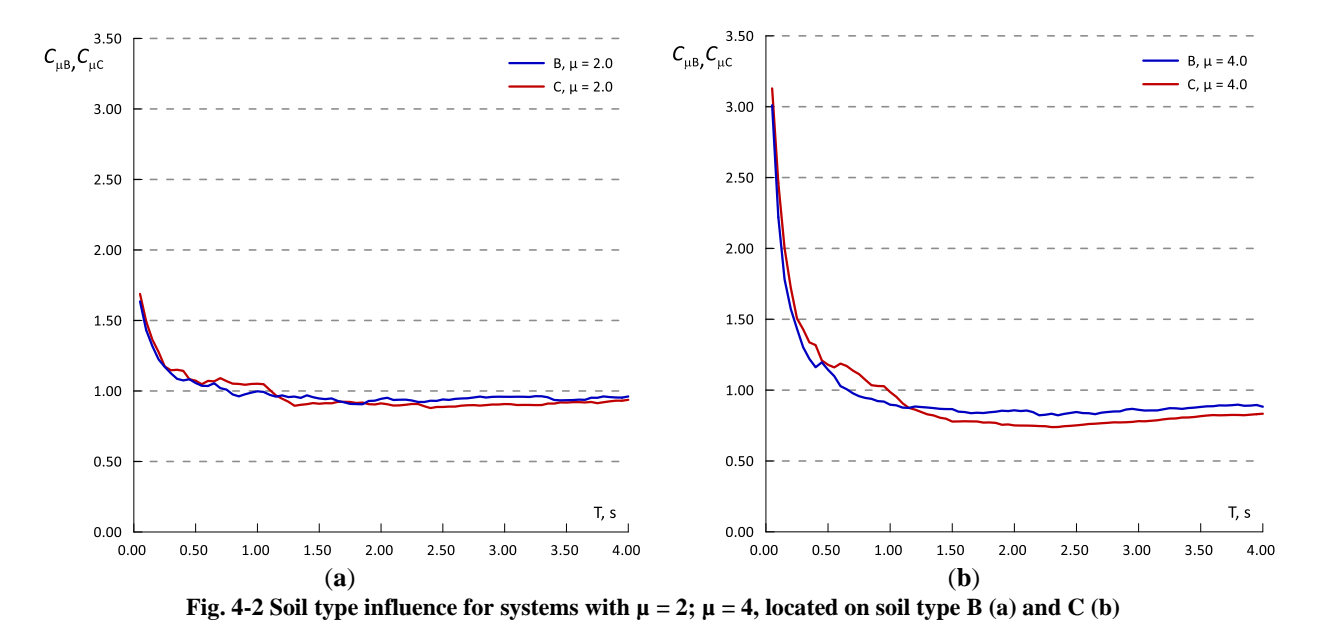
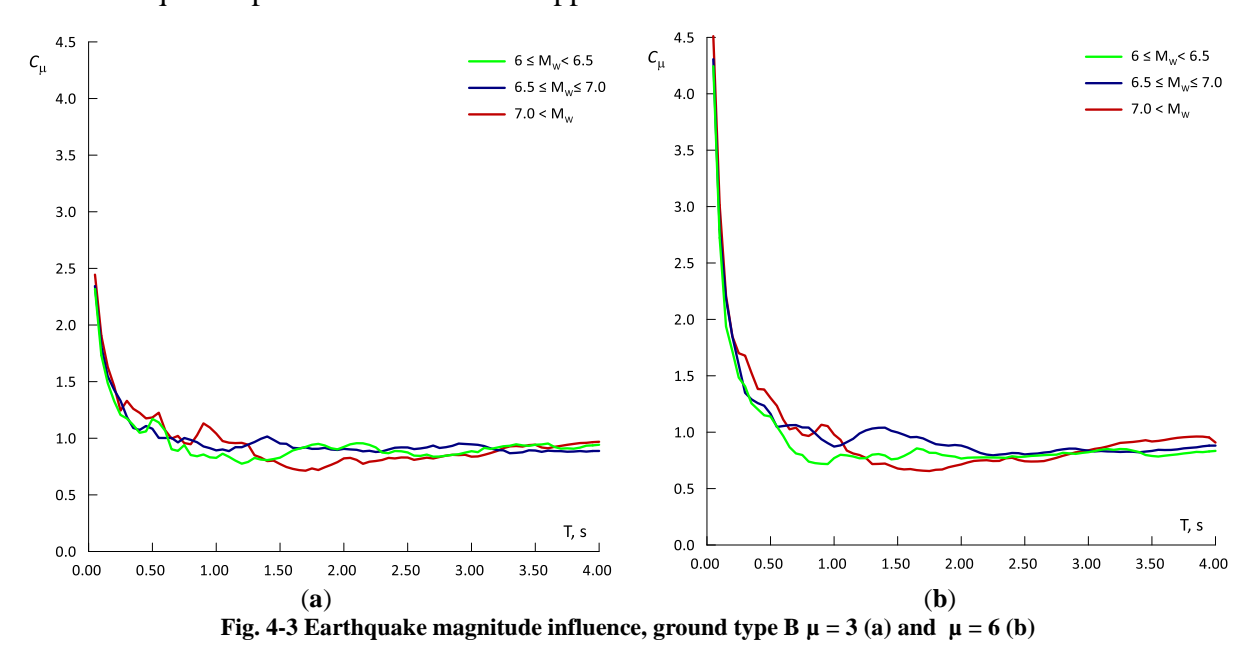


Figure 4-2 comparatively shows the variation  $C_{\mu}(T)$  for systems with limited, respectively moderate-high ductility, located on soil type B and C. Analyzing the two figures it can be concluded that inelastic systems located on ground type C have inelastic displacements higher than

those located on type B soil, up to periods of 1,20s. As expected, the difference is amplified by an increased ductility. However, for periods over 1,20s the coefficient values are approximately equal to 1,00. So, although systems located on ground type B will have higher  $C_{\mu}(T)$  values at spectral periods of more than 1,20s than their type C ground counterparts, the application of the equal displacement rule (consideration of a coefficient equal to 1,00) will lead to equal inelastic amplifications for both types of site conditions.

The most important feature of soil type influence is the change of the period from which the rule of equal displacements starts to apply. This aspect is more pronounced for systems with moderate-high ductility. Figure 4-2 shows values of 0,70s for soil type B and 1,00s for soil type C, from which the equal displacement rule can be applied.



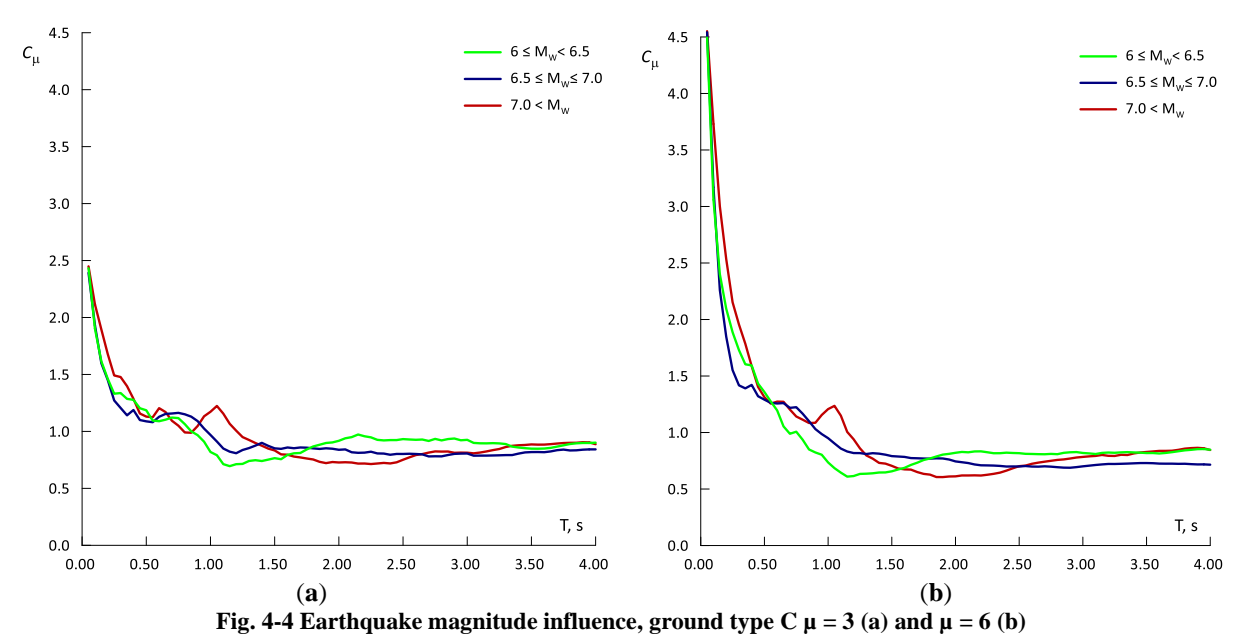
The influence of earthquake magnitude was investigated for both ground types. The recordings were ordered in three sets, depending on the magnitude: one containing records from earthquakes with magnitudes between 6,0 and 6,5, another containing recorded accelerograms during earthquakes with a magnitude between 6,5 and 7,0, the last set comprising ground motions of earthquakes with magnitudes over 7,0. The results for two displacement ductility,  $\mu = 3$  and  $\mu = 6$  are shown in Figure 4-3 for ground type B, while Figure 4-4 shows the data for type C soil.

The trend of increasing inelastic displacements is indeed present for systems with important post yield excursions (indicative,  $\mu \ge 3$ ), located on type C soil. For systems located on ground type B, the tendency to amplify the inelastic displacement requirement is recorded for a shorter range of periods.

Figure 4-4 shows the increase of  $C_{\mu}(T)$  for type C soils, for a range of spectral periods between 0,9-1,3 s. For all six ductility values for which calculations were performed, an area centered around the period of 1,10s was identified where the effect of increasing the magnitude is more pronounced, earthquakes with magnitude over 7,00 producing amplifications 30% larger than

those with  $6.5 \le Mw \le 7.00$ . This feature can have a significant impact on an inelastic design spectrum.

In order to discuss the cause of the peak near the 1,10s period on type C soil, it was necessary to investigate the characteristics of earthquake records with  $M_W > 7,0$  from the database, presented in detail in the thesis. The  $C_{\mu}(T)$  peak is a characteristic of the strong Vrancea earthquakes, the events of August 31, 1986 ( $M_W = 7,1$ ) and March 4, 1977 ( $M_W = 7,4$ ). For intermediate-depth earthquakes produced in Japan present in the database, no significant  $C_{\mu}(T)$  peaks were identified for periods over 1,00s. It should be noted that the amplifications corresponding to the strong Vrancea earthquakes of intermediate-depth are characteristic both for locations located in the city of Bucharest and its surroundings, as well as for those in the epicentral area.



The epicentral distance does not significantly influence the values of the amplification coefficient.

Examining the influence of all the factors listed above, one can distinguish the special influence of local conditions. They influence the shape of the coefficient and the period values at which it can be considered equal to unity. The magnitude of the earthquake has a significant influence on the locations located on ground type C, for a range of periods centered around the period of 1,10s.

In order to facilitate the use of the data on the amplification coefficient, a functional form has been developed to provide its median values. For a system with displacement ductility  $\mu$ , the function has the following form:

$$C_{\mu}(T) = a_1 \sqrt{T} + \frac{a_2}{T} + a_3 \ln(T)$$
 Ec. 4-2

where a<sub>1</sub>, a<sub>2</sub>, a<sub>3</sub> are coefficients obtained by regression, for each soil category and each level of displacement ductility, while T is the vibration period of the system. The first term provides the

general aspect of the function, the second calibrates the expression in the range of short periods, while the last term adjusts the allure of the function in the field of moderate-large periods.

As shown above, the earthquake magnitude can have an impact on the  $C_{\mu}(T)$  shape on type C soil. For ultimate limit state checks, it is very likely that the magnitude associated with the design seismic hazard will exceed  $M_W=7.0$ , so the effect on the coefficient must be taken into account. An additional term is added to the expression of the amplification coefficient for this type of soil. Local amplification of the inelastic displacement was considered in the form of a sinus function, which reaches its maximum amplitude at a period of 1,05 s.

$$C_{\mu}(T) = C_{\mu 1}(T) + C_{\mu 2}(T)$$
 Ec. 4-3

with:

$$C_{\mu 1}(T) = a_1 \sqrt{T} + \frac{a_2}{T} + a_3 \ln(T)$$
 Ec. 4-4

$$C_{\mu 2}(T) = 0.25 \sin \left[ \frac{\pi (T - 0.85)}{0.40} \right]$$
, for  $0.85 \le T \le 1.25$   
 $C_{\mu 2}(T) = 0$ , else

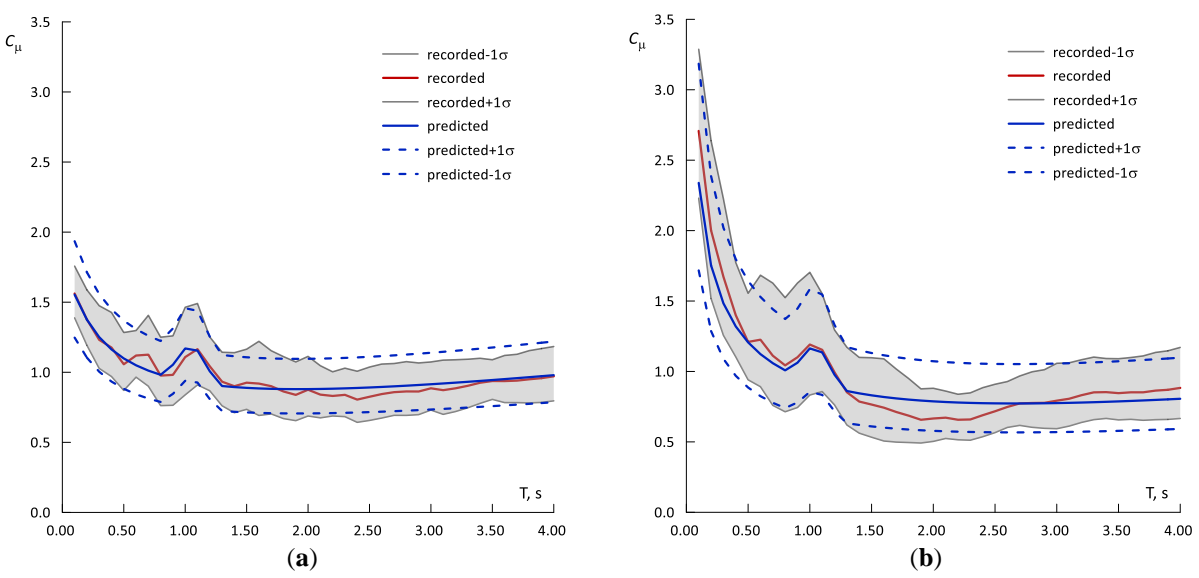


Fig. 4-5 The value of the amplification coefficient, records with  $M_W > 7$  - calculated vs. registered – ground type C,  $\mu = 2$  (a),  $\mu = 4$  (b)

By taking the value of the standard deviation  $\sigma_{C\mu(T)}$  at its mean value over the whole periods considered, the value of the coefficient  $C_{\mu}(T)$  can be obtained together with the associated variability, using only the functional form and the above tables. Examining a representation that includes only earthquakes with  $M_W > 7$ , Figure 4-5, we can see a good agreement between the values calculated using equations 4-4 and 4-5 and those obtained from the processing of records. The local peak around the 1,05s period is accurately captured, both as an average value and for the

corresponding values  $\pm 1\sigma_{C\mu(T)}$ . For systems with ductility between 1,5 and 6, the use of an average value for the standard deviation leads to conservative results for wide ranges of spectral periods. Note that the general shape of the curve, due to the term  $C_{\mu 1}(T)$  in Equation 4-4, is the same as that developed for records in the entire database. So, adding the terms  $C_{\mu 1}(T)$  and  $C_{\mu 2}(T)$  will generate values of the displacement amplification coefficient that will be in good agreement with the data processed from the records for both large magnitude earthquakes and for moderate magnitude earthquakes with a higher variability.

The displacement amplification coefficient can be used together with an elastic displacement spectrum (SD) to generate inelastic displacement spectra, which play an important role in DBD. The elastic spectrum can be a design spectrum or one developed for a seismic scenario. The design codes (MDRAP 2013; CEN 2004) provide the information needed to draw a design SD. On the other hand, using the attenuation model developed in Chapter 3 and using amplification coefficients, inelastic displacement spectra can be obtained, corresponding to a predetermined seismic scenario, described by the magnitude of the earthquake expected at the site, epicentral distance, ground conditions and (permissible) displacement ductility for design. The procedure for constructing the inelastic spectrum for a displacement ductility is simple:

- Following the disaggregation of the seismic hazard, a number of (M<sub>W</sub>, D<sub>epi</sub>) pairs results that generate the highest values of seismic amplitude on the considered site, for the average return interval considered;
- Using the GMPE presented above, the elastic displacement spectrum, SD<sub>el</sub>(T), with the associated variability is generated;
- The amplification coefficient is determined,  $C_{\mu}(T)$ , depending on the hysteretic model, the soil conditions, also together with the associated variability;
- Considering that the two variables above,  $SD_{el}(T)$  and  $C_{\mu}(T)$  are independent variables (their numerical values are not correlated), knowing the distributions of each variable (both lognormal), the inelastic displacement spectrum can be obtained as:

$$SD_{inel}(T) = SD_{el}(T) \cdot C_{il}(T)$$
 Ec. 4-6

- The product of two independent lognormally distributed variables is also lognormally distributed (Lungu & Ghiocel, 1982), with mean and standard deviation:

$$m_{\ln[SDinel(T)]} = m_{\ln[SDel(T)]} + m_{\ln[c_{\mu}(T)]}$$

$$\sigma^{2}_{\ln[SDinel(T)]} = \sigma^{2}_{\ln[SDel(T)]} + \sigma^{2}_{\ln[c_{\mu}(T)]}$$
Ec. 4-7

As mentioned above, one of the assumptions underlying the construction of the inelastic displacement spectrum is to treat  $SD_{el}(T)$  and  $C_{\mu}(T)$  as independent variables. Analyzing the correlation between the numerical values  $SD_{el}(T)$  and  $C_{\mu}(T)$  for several periods (and a limited set of data - corresponding to the earthquakes of 1977, 1986, 1990) it can be concluded that there is a weak correlation, ( $|\rho| < 0.15$ ), for some periods, or there is no correlation in the case of others. The correlation, when it occurs, is negative. This subject was also treated in the study of Ruiz-Garcia and Miranda, (2007), being highlighted a correlation coefficient that varies with the period,

usually being negative, and generally between -0.25 and 0.00. For this reason, the calculation expression of  $SD_{inel}(T)$  should be changed to:

$$SD_{inel}(T) \approx SD_{el}(T) \cdot C_{il}(T)$$
 Ec. 4-8

Below are some of the results obtained for the INCERC1977 record.

The association between the attenuation law presented in Chapter 3 and the expression of the displacement amplification coefficient are able to estimate with reasonable accuracy the inelastic spectra obtained by processing the recorded data set. For the 1977 record, in general, both components (marked with blue and green lines) are between the median values (represented by the red line) and the ones corresponding to  $\pm 1\sigma_{SDinel(T)}$ , as shown in Figure 4-6.

For the analyzed ductility values, always the major contributor for the variability of the nonlinear system response, calculated according to equation 4-7, is the elastic displacement spectrum,  $SD_{el}(T)$ . Especially for periods longer than 1,30s, the inelastic displacement demand is dominated by the elastic spectrum calculated according to the GMPE, due to equal displacements rule. There are short intervals where the inelastic spectrum corresponding to the INCERC77NS component exceeds the computed median values  $\pm 1\sigma_{SDinel(T)}$ .

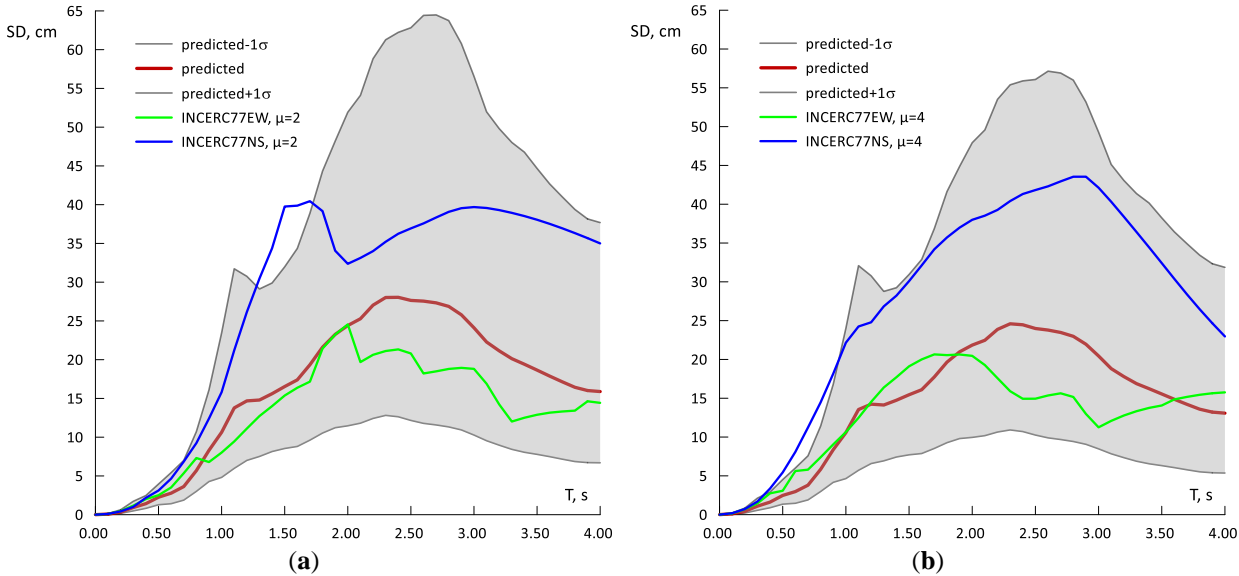


Fig. 4-6 Inelastic spectra generated for INCERC77NS and INCERC77EW vs. measured,  $\mu$  = 2 (a) and  $\mu$  = 4 (b), type C ground

## 5 Use of overdamped spectra in the analysis of the expected seismic response

The objective of this chapter is to determine if equivalent hysteretic damping can be used to describe the complex behavior during strong earthquakes of nonlinear systems. Also, it was investigated how to obtain over-damped spectra by transforming those built for 5% critical damping.

An important number of DBD procedures are focused on the concept of hysteretic damping. Equivalent linearization methods approximate the maximum response of the nonlinear behavior system with the maximum response of an equivalent linear system, with a period of vibration and viscous damping larger than that of the initial system. The researchers made significant efforts towards the improvement of equivalent linearization because it allows the analysis of the real system, with complex nonlinear behavior, using the tool of linear dynamic analysis, making the response of the system easier to understand. In addition, linearization allows the analysis of systems with nonlinear behavior in the frequency domain, the seismic excitation being specified in the design codes in the frequency domain through a smoothed response spectrum (Iwan, 2005).

The concept of equivalent viscous damping is currently used in the evaluation process of existing buildings (MBIE, 2017) and in the design of new constructions in New Zealand and the United States (Goel, 2018). It should be noted that seismic assessment of existing buildings in New Zealand is done using a simple method of lateral force analysis (SLaMA) of the capacity of the structural system involving the calculation of the displacement demand by equivalent linearization, according to the methodology described in Priestley, Calvi & Kowalsky, (2007).

Next, two models of equivalent linearization will be described and then evaluated: the one presented in (ATC-55, 2005), which uses the linearization methodology proposed by Iwan and Guyader, and the model described in Priestley, Calvi & Kowalsky (2007). It is emphasized that, although the notion of equivalent damping dates back to the 1930's and has seen significant developments in the last three decades of the same century, it is still a topic of interest, treated in the works of Wijesundara et al. (2011), Sullivan, (2016) and Grammatikou et al. (2018).

The basic concept of the equivalent linearization method used in ATC-55, (2005) is to select, subsequent to a statistical analysis, the optimal equivalent parameters for period and damping. These parameters minimize the probability of having large differences between the displacement seismic response of the nonlinear system and the equivalent one (ATC-55, 2005). This approach expands the previous studies of Iwan and Gates (1979) and Iwan (1980). The results of the latter study were evaluated along with other methods of obtaining the maximum displacement response of nonlinear systems in (Miranda & Ruiz-Garcia, 2002). The methodology proposed by Iwan gave some of the best results, the median values being close to those determined by nonlinear dynamic analysis and having low values of standard deviation. The nonlinear model used in the 1980 study was obtained using elastic elements associated with components described by Coulomb friction.

The optimal equivalent linearization parameters from (ATC-55, 2005) were obtained for three hysteretic models: bilinear, stiffness degrading and with resistance degradation. The calibration of

these parameters was done following a statistical analysis that aimed to obtain a maximum response in displacement close to that of the system with nonlinear behavior. Most previous studies have focused on minimizing the error defined as the absolute difference in the maximum displacement of the two systems: nonlinear and the equivalent elastic. Iwan (1980) argued that this approach does not necessarily leads to the best results. This is because the results of a statistical study focused on minimizing the absolute difference can lead to statistical error distributions that have zero mean but very high standard deviation. Iwan proposes to obtain equivalent period and damping values that would maximize the probability that the error would be in a range considered acceptable, from an engineering point of view. The equivalent periods thus obtained are significantly shorter than those obtained using the secant stiffness corresponding to the maximum response.

On the other hand, the equivalent linearization procedure described in Priestley, Calvi & Kowalsky (2007), is a basic component of the displacement-based design methodology developed by the three authors of the paper and benefited from the studies of Dwairi and Grant. The approach consists in calibrating the viscous damping values in such a way as to obtain equal maximum displacements on the equivalent system and on the one with nonlinear behavior. The period of the equivalent system is obtained from the secant stiffness corresponding to maximum displacement. Parameters governing the amount damping were determined for several hysteretic models (elastoplastic, bilinear, Takeda, Ramberg - Osgood). Two studies were performed, one on a large number of natural accelerograms conducted by Dwairi and one in which artificial accelerograms compatible with a spectrum performed by Grant were used. In the first study, viscous damping was calculated for each record, displacement ductility and hysteretic pattern and then the values obtained were mediated for the entire set of records. The second study aimed to obtain a damping value for which the maximum response of the equivalent and nonlinear systems are equal. The mediation was done separately on the elastic and inelastic systems, respectively, comparing the results. The two studies were initially considered zero "elastic" viscous damping. The results were very close for the Takeda model and slightly different (up to 20%) for the elasto-plastic model (Priestley, Calvi & Kowalsky, 2007).

It is worth mentioning that systems in which hysteretic energy dissipation is modeled with "thin" loops, as expected, have larger displacements than systems modeled with "fat" loops. The displacement ratio is between 1,04 and 1,08, with an average value of 1,06, regardless of the system period.

It should be noted that in the seismic assessment procedures of existing structures in New Zealand (MBIE, 2017), the values for hysteretic damping used in displacement-based calculation are very close to those in Priestley, Calvi & Kowalsky, (2007).

Next, two equivalent linearization methods are evaluated, one presented in FEMA440, based on the studies of Iwan and Guyader, and the other, based on the studies of Kowalsky, Dwairi and Grant, described in (Priestley, Calvi & Kowalsky, 2007).

The database for this study was constructed starting from the records used in the study described in Chapters 3 and 4, which aimed to obtain an attenuation model for the displacement spectrum,

respectively the construction of inelastic displacement spectra. A minimum value was set for the PGA value for this set of records because some features of weaker ground motion recordings differ significantly from strong motion recordings. For this study the PGA limit value was selected at 75cm/s², corresponding to the value of the geometric mean of the two horizontal components, according to the recommendations in (Goda & Atkinson, 2009).

The database includes 71 pairs of horizontal components (142 records) from intermediate-depth earthquakes with  $6.0 \le M_W \le 7.40$  produced in Romania, generated by Vrancea seismic source. Two recordings of an earthquake with a magnitude of 5.2 (6.10.2013) were also included, which satisfy the imposed PGA limit. After selection according to the PGA, the records were grouped according to the type of soil on which they were recorded, according to the Eurocode 8 classification. Out of a total of 71 pairs of components, 38 come from type C ground, the remaining 33 being recorded on type B soil.

For both procedures, the evaluation methodology consists of the following steps (Miranda & Ruiz-Garcia, 2002):

- 1. Determination of the displacement ductility and the vibration period of the original system, for which the maximum displacement is desired.
- 2. Calculate the period of the equivalent linear system using the equations corresponding to each equivalent linearization procedure.
- 3. Calculate the equivalent viscous damping of the linear system, depending on the displacement ductility and the hysteretic model of the original nonlinear system.
- 4. Linear dynamic analysis of the equivalent linear system having the period and damping calculated in the above steps and finding the maximum (absolute) displacement, D<sub>lin</sub>.
- 5. Comparison of the displacement thus obtained with that calculated by nonlinear dynamic calculation of the original system,  $D_{inel}$ .
- 6. Computing the relative error,  $\mathcal{E}_d = \frac{D_{lin} D_{inel}}{D_{inel}}$  (ATC-55, 2005), and then comparing it with the acceptable engineering range: -10% ... +20%.

Another way to assess the accuracy of the prediction is  $\mathcal{E}_r = \frac{D_{lin}}{D_{inel}}$ , the ratio between the

displacement of the equivalent linear system and that of the inelastic one. Values larger than one correspond to overevaluation of displacements, while subunitary values imply underestimations of the displacements of the original system.

As shown, the equivalent linearization methods presented comparatively in this study lead to different values of actual periods and damping of the equivalent system. Therefore, no predictions can be made on the results provided by the linearization methods by examining only the effective period and the equivalent damping. The comparison of the results provided by the equivalent linearization methods by evaluating the errors  $\epsilon_d$  and  $\epsilon_r$  is efficient because it directly follows the displacement of the system.

The two quantities,  $\varepsilon_r$  and  $\varepsilon_d$ , and their statistical indicators are linked (Lungu & Ghiocel, 1982) by the following:

$$\mathcal{E}_r = \mathcal{E}_d + 1$$

$$m_{\mathcal{E}_r} = m_{\mathcal{E}_d} + 1$$

$$\sigma_{\mathcal{E}_r} = \sigma_{\mathcal{E}_d}$$
Ec. 5-1

where  $m_{\epsilon r}$  and  $\sigma_{\epsilon r}$  represent the mean and standard deviation of the variable  $\epsilon_r$ . These relations allow the calculation of the statistical indicators of  $\epsilon_r$  from those calculated for  $\epsilon_d$ .

The range of periods for the oscillators is between 0,05 and 2,00s. This is due to the fact that many of the recordings of strong earthquakes are analog, and by processing them reliable results can be obtained up to periods of 4,0s. The database contains only analog records for earthquakes with  $M_W > 6,0$ . By linearization, the equivalent periods can easily exceed twice the period of the initial system, especially for high ductility values. For example, in the case of Kowalsky - Priestley linearization, the translation of the period, for a system with displacement ductility equal to five results in  $T_{eq} = T_0 \sqrt{5} = 2,23T_0$ . So, for a system with the initial period  $T_0 = 1,7s$  results  $T_{eq} = 2,23$  x 1,70 = 3,79s. To determine the maximum displacement of the system, the displacement value corresponding to the period of 3,79s must be extracted from the displacement spectrum. Due to the upper limitation of the period equivalent to 4s, the periods of the original systems must be limited to no more than approximately 2,0s.

The steps listed above have been performed for systems described by the Takeda hysteretic model with solid loops (Takeda "fat") with displacement ductility values: 1,5, 2,0, 3,0, 4,0, 5,0 and 6,0. The period of the initial systems ( $T_0$ ) was between 0,05 and 2,00 s. For each ductility level and each damping model, the parameters of the equivalent linear systems were calculated: vibration period,  $T_{eq}$  and fraction of critical damping,  $\xi_{eq}$ .

Nonlinear dynamic analyzes were performed with the USDP program (Akkar, 2016) used in a previous study, aimed at determining the maximum displacement of nonlinear systems by the coefficient method (FEMA356), described in Chapter 4. Analysis parameters: Takeda "fat" hysteretic model with unloading stiffness parameter  $\alpha = 0.3$  and post-elastic slope r = 2%, damping 5% of critical, proportional to mass.

Figure 5-1 conceptually shows the process of determining the maximum displacement using equivalent linearization, for a system with displacement ductility equal to four and the EREN86 registration, component N162.

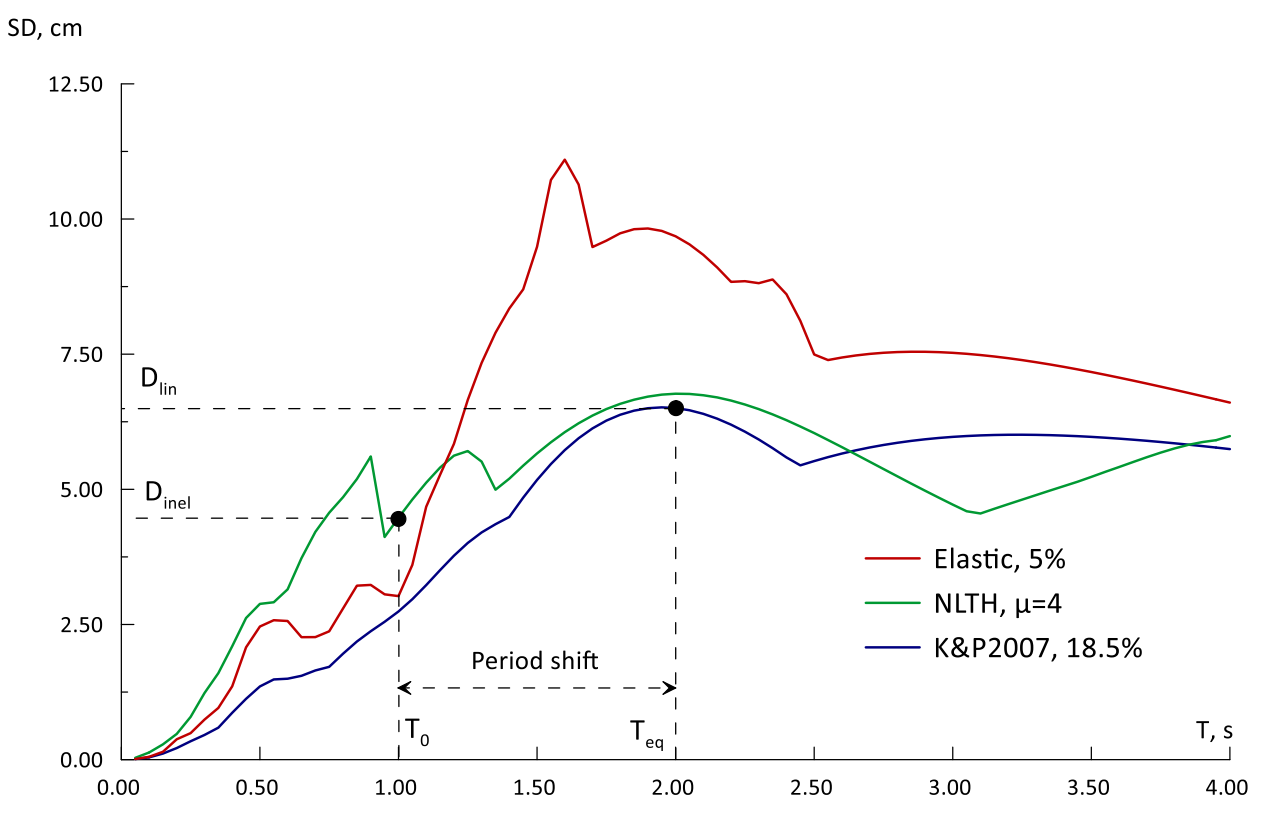


Fig. 5-1 Illustration of the evaluation methodology for equivalent linearization procedures

The elastic displacement spectrum, the inelastic spectrum and the one obtained by equivalent linearization can be represented on the same graph. The first two have the same periods on the abscissa (the periods are not translated). Instead, the spectrum of displacement obtained by equivalent linearization, corresponds to a system with a longer period than the original one (due to the phenomenon of period shift). Therefore, in order to be able to be expressed in the same coordinates (same period, initial period - of the original system), the displacement spectrum obtained by equivalent linearization must be related to the values of initial period.

For example, consider a nonlinear system having  $T_0 = 1.0s$ , with displacement ductility equal to four and zero post-elastic slope. Using the period corresponding to the secant stiffness, we obtain  $T_{eq} = T0\sqrt{4} = 2.0s$ . The displacement of the equivalent system ( $T_{eq} = 2.0s$ ) is denoted by  $D_{max}$ . Although  $D_{max}$  was recorded on the system equivalent to T = 2.0s, it corresponds to the nonlinear system with the period  $T_0 = 1.0s$ .

In this way, the elastic, inelastic and approximate displacement requirements obtained by equivalent linearization can be directly compared for any period value.

The linearization method presented in FEMA440 is an extension of the procedure developed by Iwan in the 1980s. For systems with stiffness degradation, the parameters required to calculate the characteristics of the equivalent system are tabulated. It is important to note that this equivalent linearization method can be used in displacement-based seismic design or assessment together

with an improved variant of the capacity spectrum, modified acceleration and displacement spectrum (MADRS) method (ATC-55, 2005).

The method presented in Priestley, Calvi & Kowalsky (2007), hereinafter referred to as K&P2007, considers as a equivalent period the one corresponding to the secant stiffness at the maximum seismic response. The period thus obtained is in most cases longer than that obtained from the application of the linearization procedure in FEMA440. The method has the advantage of being integrated into the displacement-based design methodology playing a key role in the formulation of Priestley, Calvi & Kowalsky (2007). For systems described by the Takeda hysteretic model with full loops (Takeda "fat"), the linearization parameters are presented in Chapter 1.

With these parameters, linear dynamic analyses were performed for the set of records in the database and the results were compared with those from the nonlinear dynamic analysis of the SDOF system.

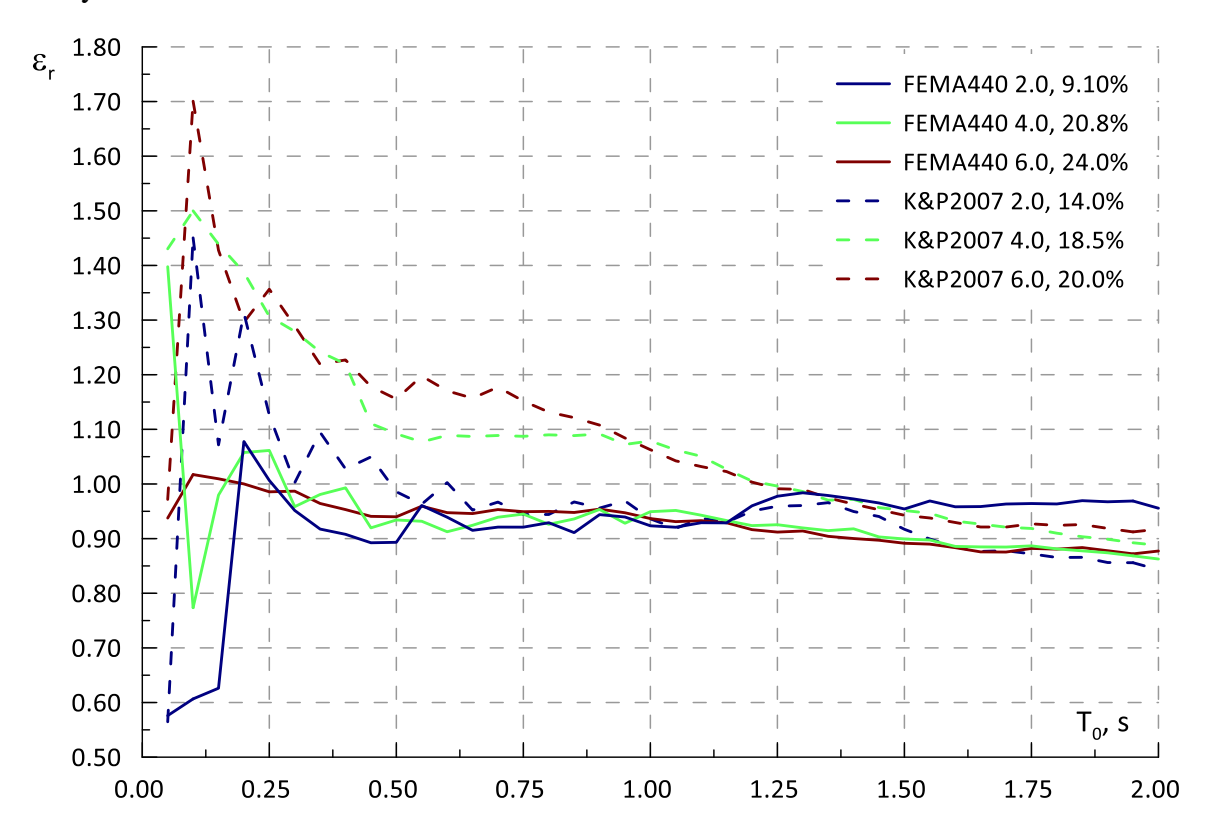


Fig. 5-2 Average values of  $\varepsilon_r$  = Dlin / Dinel, FEMA440 vs. K&P 2007

The two equivalent linearization methods presented above are currently used in the design of new constructions and in the evaluation of existing constructions. The linearization adopted in FEMA440 is used to construct the capacity spectrum for estimating the maximum displacements of nonlinear systems. The approach described in Priestley, Calvi & Kowalsky (2007) has been taken over by New Zealand assessment codes (MBIE, 2017).

To facilitate the analysis of the data generated by the two methods, the average values of the ratio  $\varepsilon_r = D_{lin}/D_{inel}$  is plotted for three values of displacement ductility, along with its standard deviation, for both damping models.

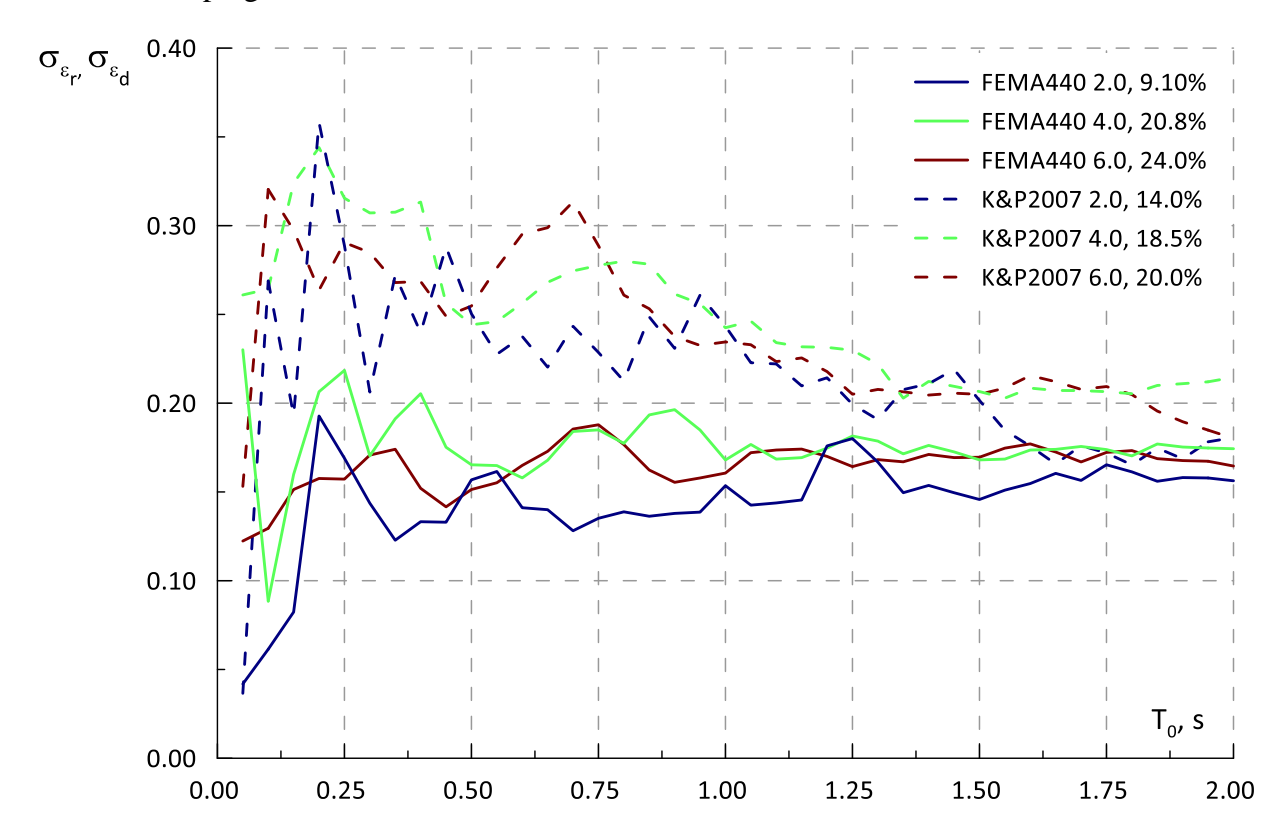


Fig. 5-3 Standard deviation of  $\epsilon r = Dlin / Dinel$ , FEMA440 vs. K&P 2007

From the visual examination of Figures 5-2 and 5-3 some conclusions can be drawn. The mean values of the displacements obtained by the linearization described in FEMA440 are very close to those of the nonlinear dynamic analysis for periods of less than 2,0 s. It can be seen that the errors,  $\varepsilon_r$ , are very small, between + 5% and -10%, for all ductilities and for periods between 0,20s and 2,00s. It is emphasized that the verification of the ability of the equivalent linearization method is done by referring to the results of the nonlinear dynamic analysis. The hysteretic model used in this study is similar (but not identical) to that used to develop relationships for equivalent linearization. Some of the differences between the values obtained by linearization and those resulting from nonlinear dynamic calculation may be caused by this fact.

The values provided by the K&P model overestimate the displacements of the nonlinear system by about 10 - 30% for periods between 0.25-1.00, after which they approach, but always remain higher than those given by FEMA for ductilities greater than 2. A clear distinction can be seen between the response of systems with  $\mu \leq 2$  and those with moderate-high ductility, systems with  $\mu = 3$  having an intermediate behavior. The former has a more predictable seismic response, with  $\epsilon_r$  errors between  $\pm$  10% over the period of 0.25-1.60s. The latter have a homogeneous response, characterized by  $\epsilon_r$  errors between  $\pm$  30% and  $\pm$  10% over the range 0.25-1.00s, and generally  $\pm$  10% between 1.00 and 2.00s. With the exception of systems with  $\mu = 1.5$ , which have a lower

standard deviation, the systems are characterized by a quasi-constant value of the standard error deviation, independent of ductility. The standard deviation is between 0,20 and 0,40, higher values being recorded in the range of 0,20-0,80s. The values are close to those obtained by Miranda in a study conducted (Miranda & Ruiz-Garcia, 2002) on a damping model developed by Kowalsky in 1994.

The variability associated with the 2007 K&P model is about 50% higher than that of FEMA for periods up to 1,0s, after which it begins to approach those provided by the US evaluation code.

The results are in good agreement with those of the study (Miranda & Ruiz-Garcia, 2002), where older variants (Iwan, 1980), (Kowalsky, 1994) of the two linearization models were evaluated. This study indicates values of  $\epsilon_r$  equal to unity for spectral periods greater than 0.5-0.6s, for systems following the Takeda hysteretic model and equivalent linearization using optimized parameters (Iwan, 1980). The Kowalsky model overestimated by up to 40% the response for short period systems, being situated in a range of  $\pm$  10% from the value of the maximum displacement obtained by nonlinear dynamic analysis for systems with periods longer than 1,0s. Regarding the standard deviation of the relative error, for elasto-plastic systems (the only hysteretic model for which variability is displayed), the Iwan model showed a standard deviation between 0,2 and 0,3 while the Kowalsky model was credited with values located between 0,25 and 0,40. The present study confirms this tendency also for systems with degrading stiffness. It is possible that a substantial part of the overestimation of the K&P 2007 method is due to ignoring a period dependent equivalent damping in Dwairi's studies, which would have led to higher equivalent damping values for systems with shorter structural periods, therefore to lower displacements and to less conservative response.

### 6 Case studies

The objective of this chapter is to apply and, subsequently validate by nonlinear dynamic analysis, design methodologies based on displacement control, considering the particular seismic hazard conditions of Romania (intermediate-depth earthquakes, large displacement demand for sites located on type C soil). This chapter mainly uses code-derived displacement spectra, but any relevant displacement spectra can be used in the displacement-based seismic design of structures. The main reason for choosing the code spectra as input data was to compare the results provided by code-based force-design with those obtained by using design methods aimed at controlling lateral displacements.

It is emphasized that in order to apply displacement-based design methodologies no calculation of the structure according to code is required. However, it must be borne in mind that the structure must be endowed with a resistance capacity at least equal to that resulting from the sizing according to the seismic design code (MDRAP, 2013).

In order to illustrate the calculation steps of displacement-based design, several case studies are presented below. They are made on three typologies of structures, often encountered in current design practice, on sites characterized according to MDRAP (2013) by design values of horizontal ground acceleration of 0,20g and 0,30g and corner periods of 0,7s, 1,0s and 1,6s. The yield and design displacement were calculated using moment-curvature bilinear idealization, using the limiting strains and the conventional lengths of the plastic joints according Priestley, Calvi & Kowalsky (2007), while the criteria for limiting the deformations were those of seismic design codes in force. The corresponding relationships from EN1998-3 (CEN, 2005) can also be used, the results of applying the two approaches may be different.

The structures chosen as case studies allow a straightforward and transparent application of displacement-based seismic calculation procedures. In the literature, (Priestley, Calvi & Kowalsky, 2007), (FIB, 2003), examples of calculation are available that deal with structures more common in the current practice of seismic design: structures with walls of different lengths or irregularly arranged and having torsional sensitivity, structures with setbacks or structures for which the interaction with the foundation ground cannot be neglected.

Nonlinear static and dynamic analysis were performed using the average values of material strengths (MDRAP, 2013), taking into account the effect of concrete confinement.

The recordings used in the dynamic calculation of the structure are artificial accelerograms, compatible with the design spectrum (Postelnicu, Damian, Zamfirescu & Morariu, 2013). In addition, the INCERC77NS accelerogram was also used.

Three types of structures were investigated: single story precast structures, buildings with reinforced concrete structural walls and buildings with dual structure (reinforced concrete walls and frames). Two types of single-story precast structures were studied, one with large clear height (H = 12.90m), the other with columns having moderate height (H = 6.00m). The first typology of precast structures was located on soils described by the current seismic code by  $a_{\rm g}=0.30{\rm g}$  and  $T_{\rm C}=1,6{\rm s}$ , respectively  $T_{\rm C}=0,7{\rm s}$ . The second typology consists of precast structures with moderate

height located on sites with  $a_g = 0.20g$  and  $T_C = 1.0s$ , respectively  $T_C = 0.7s$ . The building with structural walls, as well as the dual structure, are located in an area with  $a_g = 0.30g$  and  $T_C = 1.6s$ . A seismic code calculation was performed for all structures for reference. The structures designed according to the code were evaluated using DBD and then confirmed by nonlinear dynamic analysis. Improvements have been proposed using the Chopra & Goel DBD methodology. These were implemented, the solution being, again, verified by nonlinear dynamic analysis.

The single-story precast structures were modeled in Perform-3D (CSI, 2013) in order to assess the seismic response through nonlinear static and dynamic analysis. The characteristics of materials and plastic zones were modelled following the recommendations of Zamfirescu & Damian, (2019). Only the columns were modeled, the weight of the roof structure and the snow load being applied as forces and masses concentrated on the ends of the columns. The columns were modeled with beam elements, composed of a plastic zone and an elastic segment. The stiffness of the elastic zone was calculated using sectional analysis and it corresponds to the first yield (for calculation at ULS), according to the recommendations of Eurocode 8 (CEN, 2004). The modeling of the plastic zone at the base of the columns was done in two ways: plastic hinge ("P-M2-M3 hinge"), respectively modeling with inelastic fibers along the length of the plastic zone. The results of the two modeling techniques were close, both leading to similar results (peak displacements and internal efforts). The viscous damping was considered as Rayleigh type, the coefficients being calibrated to ensure a value of 5% of the critical damping.

The case studies for single story precast structures, having a roof that forms a rigid diaphragm, showed the following features:

- The displacement-based design methodology Chopra & Goel (2001) leads to a sizing of reinforced concrete columns that ensures compliance with the conditions of lateral stiffness imposed by the code, both for SLS and for ULS. For the considered cases, the condition of limiting drift for SLS was decisive.
- 2. The displacement ductility requirement for ULS according to P100-1/2013 is low, in all cases being below 1,60, rarely exceeding 1,50. For large height single story precast structures located on sites on firm ground (type B according to the classification EN1998-1, respectively  $T_C = 0,70$ s according to P100-1/2013), the ductility demand is even lower, below 1,20, the structures having a quasi-elastic seismic response to the action of the ULS earthquake.
- 3. The over-strength of structures, calculated with average strengths of materials, is generally in the range of 2,00 2,50. The large values are caused by the minimum reinforcement required for the concrete sections to meet the drift limitation requirements.
- 4. The ultimate hinge rotations of the columns obtained according to Priestley, Calvi & Kowalsky (2007) and those provided by EN1998-3 are close for columns with large sections (over 1000mm) while for medium-sized columns (below 650mm) the differences are over 50%, the rotations according to EN1998-3 being lower in all cases.
- 5. The second-order effects do not decisively influence the response of the structures to the corresponding ULS earthquake, as long as the limitations of the lateral displacement imposed by the code are observed. In case of non-compliance or for seismic events that

- exceed the level established by the code for ULS, the second order effects become important and can lead to significant residual deformations.
- 6. Column sectional dimensions and reinforcement obtained following the application of the DBD methodology (Chopra & Goel, 2001) are identical to those obtained from the calculation according to the code for locations located on firm ground (type B according to classification EN1998-1, respectively  $T_C = 0.70$ s according to P100-1/2013), and in some cases may be lower. For other types of site conditions, the sections of the columns resulting from the code calculation had to be adjusted in size and/or reinforcement to meet the drift limitation of the seismic design code. The difference is largely caused by the assumption adopted by the design code that the effective stiffness of the columns is half that of the gross section, regardless of detail, geometry or level of stress, while applying the DBD methodology the stiffness is assessed taking into account the variables mentioned above.

The efficiency of the DBD methodology compared to the force-based design must be assessed according to the level of fulfillment of the requirements of the seismic design code and the cost of the structure, a comparison of the basic shear forces is not conclusive (due to the use of average strength in DBD vs. design strength in seismic code design).

Regarding the value of the effective stiffness of the columns in nonlinear analyses, it is important to note that for the ULS calculations the secant stiffness at the yield was used, according to the requirements of the seismic design codes, while for SLS the secant stiffness was considered corresponding to the expected displacement at SLS. Secant stiffness at the yield was determined from sectional analysis, as recommended in (Priestley, Calvi & Kowalsky, 2007). The values obtained were compared with values from the literature. The effective stiffnesses of the columns were calculated according to Fardis (2009), ACI (2019), Elwood & Eberhard (2009), Paulay & Priestley (1992).

The building with structural walls has eight stories, the height of the ground floor being 4,00 m, while the current floors is 3,40 m, the total above-ground height being 27,80 m. The flat slab has a thickness of 25cm. In the longitudinal direction it has five bays of 8,00m and 4,50m, and in the transverse direction there are three spans of 8,00m, the total dimensions in the plan being 33,00x24,00m. At the intersection of the structural axes, 600x600mm columns are provided. They are incorporated as boundary elements in the structural walls. In the longitudinal direction are four walls with a total length of 5,10m (including the boundary elements) and a 300mm thick web. In the transverse direction there are two walls with a total length of 8,60 m, with a 300 mm thick web. The concrete is class C30/37 and the reinforcement is BST500C.

The structural wall building was modeled in Perform-3D (CSI, 2013) in order to assess the seismic response through nonlinear static and dynamic analysis. The characteristics of materials and plastic zones were modelled following the recommendations of Zamfirescu & Damian, (2019). The walls and columns were modeled, the weight of the structure being applied as forces and masses concentrated on the ends of the columns and walls. The columns were modeled with beam type elements, composed of plastic zones at the ends separated by an elastic segment. The stiffness of the elastic zone was considered half that of the gross section, due to the high level of axial stress.

The modeling of the plastic zones at the base of the columns was done with plastic hinges ("P-M2-M3 hinge"). The wall ends were modeled as bars made of inelastic fibers and the web of the structural walls was modeled with surface macroelements. They consist of three components: one for bending in plane of the wall with inelastic behavior described by fibers, a second that shapes out of the plane behavior of the wall with elastic behavior and the third that describes the behavior of the wall for shear, considered elastic. Each macroelement extends the whole floor height except for the plastic zone, where, on the height of the ground floor, two macroelements are modeled, the lower one being extended along the length of the plastic zone of the wall. The rotations in the plastic areas at the base of the walls were monitored using an extension type element ("rotation gage, wall type 4-node") available in the analysis software. The viscous damping was considered Rayleigh type, the coefficients being calibrated to ensure a value of 5% of the critical damping.

The evaluation of the structure by the DBD methodology was performed starting from several simplifying hypotheses: the slab floor does not contribute significantly to the lateral rigidity, ensures a rigid diaphragm and, on each direction, only the walls located along that direction ensure the rigidity and seismic resistance of the structure.

The analyses led to some important conclusions. An advantage of the DBD could be easily distinguished, the fact that the calculation procedure starts from an acceptable damage state, correlated with the level of hazard, the base shear resulting from this choice. Applying the DBD methodology in this case study revealed that long structural walls are desirable as they are not affected by drift limitation requirement, but by the limiting strains of concrete and reinforcement. The transverse walls in this case study had a height/length aspect of 3,25 and, for ULS, were dimensioned by the strain limits, while the longitudinal walls had an aspect of 5,45 and were governed by the drift limit imposed by code for ULS. Another advantage of long walls is that they are more rigid and, at the same design displacement, and have a higher displacement ductility, with a positive impact on the base shear. The higher the acceptable limiting strain (or ultimate rotations), the more the structure can be deformed and the displacement requirement would be reached at longer periods, which translates into lower base shears. The limit height/length ratio for which a wall is dominated by the drift limit or the limiting strains depends on the displacement demand associated with the seismic hazard at the site.

Beams have been added to the building with structural walls presented above to reduce the relative displacements, especially for SLS. Thus, frames are formed that can take over a significant fraction of the base shear. Paulay demonstrated that, for systems consisting of coupled walls, an advantageous way of distributing the effort between the components of the system can be chosen in the design phase (Paulay, 2002). Sullivan extended the scope of Paulay's procedure to dual systems consisting of connected structural walls, either only at the floor level or through link beams with reinforced concrete or steel frames (Sullivan, Priestley & Calvi, 2006).

The design procedure described in Priestley, Calvi & Kowalsky (2007) begins by assigning a fraction of the basic shear force to the frames,  $V_F = \beta_F \ V_{total}$ . It is chosen according to the dimensions of the walls and the proportion of walls-frames present on the structural plan. It is between 15% - 50%, but it is usually 30% - 35%. Also in the initial phase, the vertical distribution of the beam's strengths is chosen. Paulay indicates as favorable a constant distribution of the shear

force taken over by the frames, i.e. imposing equal bending moments at all levels, except for the last level where it should be half of that corresponding to a current level. The force related to them is applied to the last level of the structure. The shear forces distributed to the walls are obtained as the difference between the total level shear forces and the force related to the frames.

The dual building was modeled in Perform-3D (CSI, 2013) in order to assess the seismic response through nonlinear static and dynamic analysis. The characteristics of materials and plastic zones were modelled following the recommendations of Zamfirescu & Damian, (2019). The walls, wall boundary zones and columns were modeled as in the case of the wall structure. The beam elements are consisting of an elastic segment provided with moment plastic hinges at the ends. The bending stiffness of the elastic segment was considered 30% of the value corresponding to the uncracked section, according to the recommendations in ASCE (2017). The beam-column intersection was considered infinitely rigid. The rotations in the plastic zones at the base of the walls were monitored using an extension type element ("rotation gage, wall type 4-node") available in the structural analysis software. The viscous damping was considered Rayleigh type, the coefficients being calibrated to ensure a value of 5% of the critical damping.

By applying DBD methodologies, advantageous distributions of the basic shear force between the structural walls and the reinforced concrete frames can be obtained. By establishing adequate stiffnesses, frames can be assigned significant fractions (30% - 40%) of the total base shear force. At the same time, the frames drastically reduce the relative level displacements, both for ULS and for SLS. The displacement profile is close to the one estimated at the initialization of the DBD procedure, the nonlinear dynamic calculation using accelerograms compatible with the design spectrum confirming the limitation of the drifts to the proposed values. It should be noted that the rotation demand at the beam ends near the structural walls (link beams/coupling beams) is important and can be an important factor in sizing the dual structure.

The redistribution of shear forces from walls to frames, after reaching the wall yielding, was highlighted by nonlinear static calculations and is in agreement with the allocation of forces between the two subsystems chosen by the DBD methodology. By applying the Chopra & Goel (2001) methodology, more economical solutions can be obtained than those resulting from the calculation with seismic forces of code.

### 7 Conclusions

#### 7.1 Personal contributions

From the studies carried out, the following significant contributions are highlighted:

a) The development of a GMPE for the displacement spectrum of Vrancea subcrustal earthquakes. Emerged following a study on the displacement spectra of crustal (Banat) and intermediate-depth (Vrancea) earthquakes, the GMPE allows obtaining ordinates for spectral periods between 0,10s and 4,00s using three key parameters: earthquake magnitude, soil type (classification according to EN1998) and epicentral distance. The ground motion model is applicable to areas outside the Carpathian Arch: Moldova, Muntenia and Dobrogea, for locations located at epicentral distances between 30 and

300km, on type B or C soil. It successfully describes seismic events and for given seismic scenarios can provide data input to apply design methodologies based on displacement control.

The GMPE was developed using a database containing 272 records (544 horizontal components) generated by 15 intermediate-depth earthquakes. The study revealed the important influence of magnitude and soil conditions on the shape and amplitude of deformations. Earthquakes with large magnitudes produce large amplifications on type C ground, especially for spectral periods exceeding 1,20s. The epicentral distance has a smaller effect on the ordinates, generally the amplitude decreasing by 1/3 for every 50km. Increasing the magnitude, or decreasing the epicentral distance, leads to the narrowing of the area with large amplifications, for moderate magnitudes (Mw <7,0) there is a tendency to form a plateau area for periods longer than 2,00s.

The GMPE was successfully tested, according to relevant literature, by evaluating the interevent and intra-event residues.

This study was disseminated by participating at 16<sup>th</sup> European Conference on Earthquake Engineering, an international workshop and by publishing an article in an ISI-rated journal.

b) Development of an empirical expression of the coefficient of amplification of elastic displacement,  $C_{\mu}(T)$ , for new reinforced concrete structures, obtained after conducting a study on the displacement demand of inelastic reinforced concrete systems subjected to the action of intermediate-depth earthquakes. Direct determination of the coefficient according to the displacement ductility was preferred in order to avoid the introduction of additional approximations. The coefficient  $C_{\mu}(T)$  can also be used together with design displacement (code) spectra to generate inelastic design spectra.

The effects of magnitude, epicentral distance and soil type were considered on the inelastic displacement demand of new reinforced concrete structures following Takeda model, with stiffness degradation. Again, the earthquake magnitude and the soil type have the greatest influence on the inelastic amplifications of the displacement response. A local peak was identified around the periods 0.90-1.20s, present for earthquakes with  $M_W>7.0$  for locations located on type C ground. This peak is related to the frequency content of strong Vrancea earthquakes and is incorporated in the empirical expression of  $C_{\mu}(T)$ .

By using the GMPE for spectral displacements and the expression of the displacement amplification coefficient, inelastic displacement spectra can be obtained for a given seismic scenario, which contain both the variability associated with the attenuation model and that due to inelastic behavior. In general, the uncertainty related to the GMPE (elastic displacement requirement) is what determines the largest variability of the total response of the inelastic system. Uncertainty caused by inelastic amplifications has a higher weight only for systems with high ductility,  $\mu_{\Delta} > 4$ , and for structural period of less than 1,5 s.

This study was disseminated by publishing an article in an ISI-rated journal.

c) A study on the modeling of energy dissipation by hysteretic damping was carried out, starting from harmonic vibrations and then assessing the existing models which describe the seismic response. Motivation was determined by the extensive use of this method of quantifying energy dissipation in displacement-based design procedures (Priestley, Calvi

& Kowalsky 2007) or displacement-based seismic assessment (ATC40, 1996) (MBIE, 2017).

Two equivalent linearization models were evaluated for Takeda hysteretic rule responding systems with stiffness degradation: Iwan & Guyader in FEMA440 (ATC-55, 2005) and Kowalsky & Priestley (Priestley, Calvi & Kowalsky 2007). The first equivalent linearization method leads to accurate estimates of the seismic displacement response, the errors being generally below 10%. Being a method that aims to provide optimal damping values and equivalent period, it is more difficult to integrate it in the classical framework of displacement-based design, but can be used in the modified capacity spectrum method (MADRS) (ATC-55, 2005), which goes beyond the scope of this paper.

The Kowalsky & Priestley linearization method leads to accurate estimates of inelastic system displacements for systems with  $\mu_{\Delta} \le 2$ . For systems with moderate or high ductility, the method provides conservative results (+10% ...+30%) for periods of no more than 1,0s, after which the results are closer to those of the nonlinear dynamic analysis ( $\pm$  10%).

The mode of conversion of the response spectra from the conventional viscous damping value of 5% to higher damping values was also evaluated. It was found that the models proposed in EN1998 (CEN, 2004) and FEMA440 (ATC-55, 2005) lead to very close results for periods larger than 0.25s, and that the observed data are well approximated by the two models.

d) Application of the DBD Chopra & Goel (2001) methodology to a number of typologies of structures, located in areas described according to P100-1/2013 by a<sub>g</sub> = 0,20g or a<sub>g</sub> = 0,30g. Each structure was dimensioned according to the seismic design code P100-1/2013 to create a reference frame, then, dimensions or reinforcement were proposed according to the DBD methodology, having as input data the design spectrum corresponding to each location. The seismic performance of the two solutions was evaluated by nonlinear dynamic analysis, using for this purpose a suite of accelerograms compatible with the design spectrum.

For the first structural type, large height precast single-story structures located in seismic areas with  $a_g = 0.30$  g, low displacement ductility requirements were highlighted, generally below 1,50. The drift limitation condition at SLS dictated the dimensions of the columns, resulting in a low level of compression which led in the calculations according to DBD procedures to lower stiffness values in the cracked stage than those established in the code. This leads to differences between the reinforcement amount for the sections designed according to the code, respectively according to DBD with the consideration of the secant stiffness corresponding to the expected drift at SLS. The differences are important for sites located in areas described by  $T_C = 1.6s$  and are insignificant for sites located on soil type with  $T_C = 0.7s$ . For sites with  $T_C = 0.7s$ , the DBD can lead to lower reinforcement coefficients than those required by the code. For this type of structure, second-order effects can be important and must be evaluated in the case of slender columns. An abnormal design situation was also investigated, in case no restrictions are imposed on the limitation of lateral movements to SLS or ULS, the only condition imposed was the limitation of rotations in plastic hinges to the values for the performance level "limitation of degradation". The structure thus dimensioned showed an increased sensitivity to second

order effects and recorded significant residual deformations for some seismic movements considered.

The moderate height precast single-story structures, located in seismic areas with  $a_g = 0.20g$ , display a similar behavior to their large height counterparts. The structures located on sites described by  $T_C = 1.0s$ , analyzed by DBD procedures require larger sections or stronger reinforcements than those established according to the code calculation, in order to meet the drift limitation at SLS. As mentioned for large height single-story structures, for sites with  $T_C = 0.7s$ , the application of DBD can lead to lower reinforcement amounts than those required by the code.

In the case of structural walls buildings, the design according to DBD leads to more economical solutions in the case of long walls than the code seismic design. For short walls, the amount of reinforcement required to meet the drift limitation conditions at ULS is larger than that established according to the code. Walls classified as long have the ratio between the height of the wall and the height of the section (aspect) set in such a way that material strains govern the design at ULS. For the seismic site conditions studied ( $a_g = 0.30g$ ,  $T_C = 1.6s$ ) and using the limit unitary deformations from Priestley, Calvi & Kowalsky (2007), the value of the aspect ratio is in the range of 3.0 - 3.5.

In the case of dual structures, for the same location conditions as the wall structures described above, the DBD methodologies offer advantageous distributions of the base shear between the structural walls and the reinforced concrete frames. By establishing appropriate stiffnesses, frames can be assigned significant fractions of the total base shear from the beginning of the design process, even if the elastic analysis indicates a different distribution of forces between the frames and the structural walls. Thus, more economical solutions can be obtained than those obtained from the seismic code design. The frames proportioned this way drastically reduced the relative level displacements, both for ULS and for SLS. The redistribution of shear forces from walls to frames, after reaching the wall yield displacement has been highlighted by nonlinear static calculations and is in agreement with the allocation of forces between the two subsystems chosen by the DBD methodology.

In addition to these contributions, bibliographic studies and investigations on the current state of knowledge are added for all chapters 1 - 5.

In view of the above, the major objectives of the scientific research program can be considered to have been met.

### 7.2 Recommendations for future research

Several future directions for research were distinguished:

- Development of a GMPE for the spectral displacement that includes as a predictive variable the focal depth, including the new classification of soil conditions proposed in Pitilakis, Riga & Anastasiadis (2013);
- Determining the values of the coefficient  $C_{\mu}(T)$  for other hysteretic models, characteristic of some reinforced concrete structural systems (bridge piers, prestressed frames, isolators) or steel structures;

- Analysis from a displacement-based design perspective of torsion sensitive structures;
- Investigate the optimal distribution of the basic shear force in the case of walls of different lengths;
- Development of an evaluation procedure based on displacement control for seismic assessment of existing structures.

### 8 Published articles

Vacareanu, R., Olteanu, P., Chesca, A. (2006). Seismic Fragility of High-Rise RC Moment-Resisting Frames. Estimation of Drift Hazard. Proceedings of The First European Conference on Earthquake Engineering and Seismology. Geneva, Switzerland, 3-8 September 2006;

Kope, F., Onofrei, C., Olteanu, P. (2012) - Hazard Seismic si Performanta. AICPS Review 1-2/2012, 88-102;

Kope, F., Onofrei, C., Olteanu, P. (2012) - Statistical Distributions for Probabilistic Seismic Hazard Analysis. Revue Roumaine des Sciences Techniques - Série de Mécanique Appliquée, Tome 57, N° 1, P. 85–99, Bucharest, 2012;

Kope, F., Onofrei, C., Olteanu, P. (2014) - Determinarea fragilităților seismice considerând moduri de cedare multiple prin calcul static neliniar multimodal. AICPS Review 1-2/2014, 162-171;

Olteanu, P., Colibă, V., Văcăreanu, R., Pavel, F., Ciuiu, D. (2016). Analytical seismic fragility functions for dual RC structures in Bucharest. În R. Văcăreanu & C. Ionescu. (Ed.), The 1940 Vrancea Earthquake. Issues, Insights and Lessons Learnt. Proceedings of the Symposium Commemorating 75 Years from November 10, 1940 Vrancea Earthquake (pg. 463-480). Springer Natural Hazards Book Series. doi:10.1007/978-3-319-29844-3;

Olteanu, P., Vacareanu, R. (2018). Spectral Displacement Prediction Equations for Vrancea Intermediate-Depth Seismic Source. Proceedings of the 16th European Conference of Earthquake Engineering, Thessaloniki 18 – 21 June 2018;

Olteanu, P., Vacareanu, R. (2020). Ground Motion Model for Spectral Displacement of Intermediate-Depth Earthquakes Generated by Vrancea Seismic Source. Geosciences MDPI, 10(8). doi.org/10.3390/geosciences10080282;

Olteanu, P., Vacareanu, R. (2021). Inelastic displacement demand of RC buildings subjected to earthquakes generated by intermediate-depth Vrancea seismic source. Natural Hazards, 109, 2509-2534. doi:10.1007/s11069-021-04930-3;

Olteanu, P., Vacareanu, R. (in press). Seismic input for displacement-based design of RC buildings in Romania. 3rd European Conference on Earthquake Engineering & Seismology, Bucharest, Romania, 2022.

### References

- ACI. (2019). Building Code Requirements for Structural Concrete (ACI 318-19). Farmington Hills, MI, USA: American Concrete Institute.
- Akkar, S. (2016, Noiembrie 28). *Utility Software for Data Processing*. Preluat de pe USDP: http://web.boun.edu.tr/sinan.akkar/usdp1.html
- Aldea, A. (2013). Seismic motions Examples of application in earthquake engineering. (A. Aldea, Ed.) Bucharest: Matrix Rom.
- ASCE. (2017). ASCE/SEI, 41-17 Seismic Evaluation and Retrofit of Existing Buildings. Reston, Virginia: American Society of Civil Engineers.
- ATC-40. (1996). *Seismic evaluation and retrofit of concrete buildings*. Redwood City, California: Applied Technology Council.
- ATC-55, A. T. (2005). *FEMA440, Improvement of Nonlinear Static Seismic Analysis Procedures*. Washington, D.C.: Federal Emergency Management Agency.
- Blandon, C. A. (2004). *Equivalent Viscous Damping Equations for Direct Displacement Based Design*. Pavia: European School of Advanced Studies in Reduction of Seismic Risk.
- Boore, D., Joyner, W., & Fumal, T. (1997). Equations for Estimating Horizontal Response Spectra and Peak Acceleration from Western North American Earthquakes: A Summary of Recent Work. *Seismological Research Letters*, 128-153.
- Cauzzi, C., & Faccioli, E. (2008). Broadband (0.05 to 20 s) prediction of displacement responsespectra based on worldwide digital records. *Journal of Seismology*, 12, 453-475.
- CEN. (2004). European Standard EN 1998-1:2004 Eurocode 8: Design of structures for earthquake resistance, Part 1: General rules, seismic actions and rules for buildings. Brussels: Comite Europeen de Normalisation.
- CEN. (2005). European Standard EN 1998-3:2005 Eurocode 8: Design of structures for earthquake resistance, Part 3: Assessment and retrofitting of buildings. (ed. 2005). Brussels: Comite Europeen de Normalisation.
- CEN. (2005b). European Standard EN 1998-3:2005 Eurocode 8: Design of structures for earthquake resistance Part 2: Bridges. Brussels: Comite Europeen de Normalisation.
- Chopra, A. K., & Goel, R. K. (2001). Direct Displacement-Based Design: Use of Inelastic Design Spectra Versus Elastic Design Spectra. *Earthquake Spectra*, 17(1), 47-64. doi:10.1193/1.1586166
- CSI. (2013). Perform-3D Version 5.0.1. Computers and Structures, Berkeley, California.
- Damian, I. (2014). *Aplicarea metodelor bazate pe deplasare la proiectarea seismică a structurilor de hale parter cu stâlpi în consolă de beton armat.* București: Teză de doctorat, UTCB.

- Elwood, K., & Eberhard, M. (2009). Effective Stiffness of Reinforced Concrete Columns. *ACI Structural Journal*, 106(4), 476-484.
- Fardis, M. (2009). Seismic Design, Assessment and Retrofitting of Concrete Buildings Based on EN-Eurocode 8. Dordrecht: Springer Netherlands.
- FEMA-356. (2000). *Prestandard and commentary for the seismic rehabilitation of buildings.* American Society of Civil Engineers, Reston.
- FIB. (2003). *Displacement-based seismic design of reinforced concrete buildings*. Lausanne, Switzerland: International Federation for Structural Concrete (FIB).
- Goda, K., & Atkinson, G. (2009). Seismic Demand Estimation of Inelastic SDOF Systems for Earthquakes in Japan. *Bulletin of the Seismological Society of America*, 3284–3299.
- Goel, R. (2018). Evaluation of a Substitute Structure Method to Estimate Seismic Displacement Demand in Piers and Wharves. *Earthquake Spectra*, *34*(2), 759-772.
- Grammatikou, S., Fardis, M., & Biskinis, D. (2018). Hysteretic Damping in Reinforced Concrete Members and Structures. *16th European Conference on Earthquake Engineering 18-21 June 2018*. Thessaloniki.
- Hassani, N., Amiri, G., Bararnia, M., & Sinaeian, F. (2017). Ground motion prediction equation for inelastic spectral displacement in Iran. *Scientia Iranica*, 24, 164-182.
- Iwan, W. (1980). Estimating Inelastic Response Spectra from Elastic Spectra. *Earthquake Engineering and Structural Dynamics*, 8, 375-388.
- Iwan, W., & Gates, N. (1979). The Effective Period and Damping of a Class of Hysteretic Structures. *Earthquake Engineering and Structural Dynamics*, 7, 199-211.
- Joyner, W., & Boore, D. (1993). Methods for Regression Analysis of Strong-Motion Data. *Bulletin of the Seismological Society of America*, 469-487.
- Joyner, W., & Boore, D. (1994). Errata Methods for Regression Analysis of Strong-Motion Data. Bulletin of the Seismological Society of America, 955-956.
- Kanno, T., Narita, A., Morikawa, N., Fujiwara, H., & Fukushima, Y. (2006). A new attenuation relation for strong ground motion in Japan based on recorded data. *Bulletin of Seismological Society of America*, 96, 879-897.
- Lungu, D., & Ghiocel, D. (1982). *Metode Probabilistice în Calculul Construcțiilor*. București: Editura Tehnică.
- MBIE. (2017). The Seismic Assessment of Existing Buildings. Technical Guidelines for Engineering Assessments. Ministry of Business, Innovation and Employment, Earthquake Commission, New Zealand Society for Earthquake Engineering, Structural Engineering Society and the New Zealand Geotechnical Society. Retrieved from ww.EQ-Assess.org.nz

- MDRAP. (2013). *P100-1/2013*. București, România: Ministerul Dezvoltării Regionale și a Administrației Publice.
- Miranda, E. (2001). Estimation of inelastic deformation demands of SDOF systems. *Journal of Structural Engineering*, 127(9), 1005-1012.
- Miranda, E., & Ruiz Garcia, J. (2003). Inelastic displacement ratios for evaluation of existing structures. *Earthquake Engineering and Structural Dynamics*, 32, 1237-1258.
- Miranda, E., & Ruiz-Garcia, J. (2002). Evaluation of approximate methods to estimate maximum inelastic displacement demands. *Earthquake Engineering and Structural Dynamics*, 539-560.
- Neagu, C., Arion, C., Aldea, A., Văcăreanu, R., & Pavel, F. (2017). Ground Types for Seismic Design in Romania. 6th National Conference on Earthquake Engineering & 2nd National Conference on Earthquake Engineering and Seismology Proceedings (pg. 345-352). București: Publishing Conspress.
- Olteanu, P., & Vacareanu, R. (2020). Ground Motion Model for Spectral Displacement of Intermediate-Depth Earthquakes Generated by Vrancea Seismic Source. *Geosciences MDPI*, 10(8). doi:https://doi.org/10.3390/geosciences10080282
- Olteanu, P., & Vacareanu, R. (2021). Inelastic displacement demand of RC buildings subjected to earthquakes generated by intermediate-depth Vrancea seismic source. *Natural Hazards*, 109, 2509-2534. doi:https://doi.org/10.1007/s11069-021-04930-3
- Paulay, T. (2002). The displacament capacity of reinforced concrete coupled walls. *Engineering Structures*, 24, 1165-1175.
- Paulay, T., & Priestley, M. (1992). Seismic Design of Reinforced Concrete and Masonry Buildings. John Wiley & Sons, Inc. doi:10.1002/9780470172841
- Pitilakis, K., Riga, E., & Anastasiadis, A. (2013). New code site classification, amplification factors and normalized response spectra based on a worldwide ground-motion database. *Bulletin of Earthquake Engineering*, 11(2013), 925–966. doi:10.1007/s10518-013-9429-4
- Postelnicu, T., Damian, I., Zamfirescu, D., & Morariu, E. (2013). *Proiectarea structurilor de beton armat în zone seismice*. (T. Postelnicu, Ed.) București: MarLink.
- Priestley, M. (2003). *Myths and Fallacies in Earthquake Engineering Revisited* (ed. The Ninth Mallet Milne Lecture, 2003). Pavia, Italia: Rose School.
- Priestley, M., & Kowalsky, M. (2000). Direct Displacement-Based Seismic Design of Concrete Buildings. *Bulletin of The New Zealand Society for Earthquake Engineering*, 33(4), 421-444.
- Priestley, M., Calvi, G., & Kowalsky, M. (2007). *Displacement-Based Seismic Design Of Structures*. Pavia, Italy: IUSS Press.

- Priestley, N., & Calvi, M. (1997). Seismic Design Methodologies for the Next Generation of Codes. (P. Fajfar, & H. Krawinkler, Ed.) London. doi:10.1201/9780203740019
- Ruiz-Garcia, J., & Miranda, E. (2007). Probabilistic estimation of maximum inelastic displacement demands for performance-based design. *Earthquake Engineering and Structural Dynamics*, *36*, 1235–1254.
- Shibata, A., & Sozen, M. (1974). The Substitute-Structure Method For Earthquake-Resistant Design of RC Concrete Frames. Urbana, Illinois: Engineering Studies, University of Illinois.
- Strong Motion Seismograph Networks (K-NET, KiK-net). (2017, Ianuarie 30). Preluat de pe National Research Institute for Earth Science and Disaster Resilience: http://www.kyoshin.bosai.go.jp/
- Sullivan, T. (2016). Guidance on the use of equivalent viscous damping for seismic assessment. Proceedings of the 2016 New Zealand Society for Earthquake Engineering Conference, Christchurch, 1-3 April 2016, (pg. Paper No. O-27).
- Sullivan, T., Priestley, N., & Calvi, G. (2006). Direct Displacement-Based Design of Frame-Wall Structures. *Journal of Earthquake Engineering*, 10(Special Issue 1), 91-124.
- Takeda, T., Sozen, M., & Nielsen, N. (1970). Reinforced concrete response to simulated earthquakes. *Journal of Structural Division*, 96(12), 2257-2273.
- Vacareanu, R., Demetriu, S., Lungu, D., Pavel, F., Arion, C., Iancovici, M., . . . Neagu, C. (2014). Empirical ground motion model for Vrancea intermediate-depth seismic source. *Earthquakes and Structures*, 6, 141-161.
- Vacareanu, R., Radulian, M., Iancovici, M., Pavel, F., & Neagu, C. (2015). Fore-Arc and Back-Arc Ground Motion Prediction Model for Vrancea Intermediate Depth Seismic Source. *Journal of Earthquake Engineering*, 19:3, 535-562.
- Văcăreanu, R., Pavel, F., Aldea, A., Arion, C., & Neagu, C. (2015). *Elemente de analiză a hazardului seismic*. București: Conspress.
- Wijesundara, K., Nascimbene, R., & Sullivan, T. (2011). Equivalent viscous damping for steel concentrically braced frame structures. *Bulletin of Earthquake Engineering*, *9*, 1535–1558. doi:doi.org/10.1007/s10518-011-9272-4
- Zamfirescu, D., & Damian, I. (2019). Verificarea prin calcul a comportării neliniare pentru structuri cu pereți de beton armat. *Curs online, Asociația Inginerilor Constructori Projectanți de Structuri*.